

The impact of glasma on heavy flavor azimuthal correlations and spectra

Dana Avramescu,^{1,2,*} Vincenzo Greco,^{3,4,†} Tuomas Lappi,^{1,2,‡} Heikki Mäntysaari,^{1,2,§} and David Müller^{5,¶}

¹*Department of Physics, University of Jyväskylä,*

P.O. Box 35, 40014 University of Jyväskylä, Finland

²*Helsinki Institute of Physics, P.O. Box 64, 00014 University of Helsinki, Finland*

³*Department of Physics and Astronomy, University of Catania, Via S. Sofia 64, I-95123 Catania*

⁴*INFN-Laboratori Nazionali del Sud, Via S. Sofia 62, I-95123 Catania, Italy*

⁵*Institute for Theoretical Physics, TU Wien, Wiedner Hauptstraße 8, A-1040 Vienna, Austria*

We study the phenomenological impact of the pre-equilibrium glasma initial stage of heavy-ion collisions on heavy quark azimuthal correlations and spectra. Using our numerical solver, we simulate the transport of heavy quark test particles in an SU(3) glasma background field. The glasma field equations are formulated using classical real-time lattice gauge theory, and the heavy quark dynamics are described by classical transport equations numerically solved using the colored particle-in-cell method. For the first time, the effect of the glasma stage on the azimuthal correlations of $c\bar{c}$ and $b\bar{b}$ pairs is studied. The resulting azimuthal width $\sigma_{\Delta\phi}$ exhibits a large and quick decorrelation due to the strong glasma fields. Further, we evaluate how the p_T -broadening in the glasma affects heavy quark p_T -spectra, which are initialized according to the FONLL heavy quark production calculation. The nuclear modification factor R_{AA} is extracted for c and b quarks in the glasma and additional nuclear PDF effects accounting for gluon shadowing are included.

CONTENTS

References

17

I. Introduction	1
II. Framework	3
A. Glasma fields	3
B. Test particles	4
III. Computing observables	5
A. Two-particle correlations	5
B. Nuclear modification factor	6
1. Numerical R_{AA} (glasma simulations)	8
2. Analytical R_{AA} (toy model)	8
IV. Results	8
A. Numerical parameters	9
B. Two-particle correlations	10
C. Nuclear modification factor	10
1. Numerical R_{AA} (glasma simulations)	10
2. Analytical R_{AA} (toy model)	14
V. Conclusion	15
Acknowledgments	16
A. Classical Casimir invariants	16
1. Casimir scaling	16
2. Effect of cubic Casimir	17
a. Momentum broadening	17
b. Decorrelation width	17

I. INTRODUCTION

Ultra-relativistic heavy-ion collisions (HICs) are experimentally studied with the Large Hadron Collider (LHC) and the Relativistic Heavy Ion Collider (RHIC). They provide the extreme temperature and density conditions necessary to produce the Quark Gluon Plasma (QGP), a medium consisting of deconfined quarks and gluons [1, 2]. It has been a long-standing difficulty to understand the intricate space-time dynamics of the produced medium. Its properties may not solely be described using directly Quantum Chromodynamics (QCD). The evolution of the bulk medium can be viewed as a stage-by-stage process, where each stage is characterized using an effective model. The standard approach is to use an initial pre-equilibrium stage, followed by a kinetic theory description coupled to relativistic hydrodynamics, which then undergoes particlization and hadronization [3–8]. This description of HICs, together with bayesian analysis [9–11], have been successful at reproducing experimental data and extracting bulk properties of the QGP. An alternative way to infer the features the medium created in HICs is to study hard probes, such as heavy quarks and jets [12–20]. Due to their special kinematic regimes, namely large mass for heavy quarks and high energy for jets, they are “separated” from the underlying bulk medium and may probe its properties. Additionally, since the hard probes are produced early in the collision, they experience the whole evolution of the QGP and, most intriguingly, can be influenced by the initial stage [21, 22]. The early stage of HIC may be described using the Color Glass Condensate (CGC) [23–27] effective field theory. Within CGC, high-energy nuclei generate gluon fields which are treated as classical. The collision of CGC

* Corresponding author: dana.d.avramescu@jyu.fi

† greco@lns.infn.it

‡ tuomas.v.v.lappi@jyu.fi

§ heikki.mantysaari@jyu.fi

¶ dmueller@hep.itp.tuwien.ac.at

nuclei produces the glasma [27–30], an over-occupied gluonic medium consisting of strong color fields. The glasma can be expected to have a significant effect on the transport of the hard probes.

Many recent studies have investigated the impact of the pre-equilibrium stage of HICs on the properties of heavy quarks and jets. The classical transport of heavy quarks in the glasma stage was explored in [31–40] and showed to exhibit a different behaviour compared to the diffusion models applicable in the QGP phase [15, 16, 41, 42]. The jet momentum broadening in the glasma was extracted for eikonal jets from glasma lattice field correlators [43, 44], revealing a large jet transport coefficient. Similarly large transport coefficients were obtained using an analytical framework where the glasma fields are treated in the proper time expansion [45–49]. The heavy quark and jet transport coefficients for hard probes in glasma were extracted from colored particle-in-cell simulations [50, 51] and confirmed the large values previously obtained.

After the glasma stage, hard probes were studied in pre-equilibrium by using QCD effective kinetic theory (EKT). The values for the heavy quark and jet transport coefficients were shown to be compatible with the large values obtained in the glasma [52–54]. In [55], the heavy quark drag and diffusion coefficients were extracted in the pre-equilibrium stage and in [56] the thermalization of minijets in an expanding non-equilibrium QGP background was investigated. The heavy quark diffusion coefficient in the infinite mass limit was obtained from lattice field correlators in an over-occupied gluonic plasma resembling the glasma in [57–60]. The heavy quark momentum broadening was extracted for heavy quarks with finite masses from real-time lattice simulations for a highly occupied non-Abelian plasma in [61]. The impact of anisotropy, a feature inherent to the pre-equilibrium stage, was studied in [62–66] for the momentum broadening, quenching and polarization of jets in intermediate stages of HICs.

Energy loss in the glasma was first addressed in [67] and jet energy loss from synchrotron radiation was evaluated in [68] using an analytical description of the glasma electric flux tubes. Beyond the glasma stage, energy loss in the pre-equilibrium phase was investigated using various theoretical descriptions. In [69], within the EKRT framework [70] which implements a pQCD-based initial stage model coupled to hydrodynamics, it was shown that the energy loss in the early stage is suppressed. A variant of the Baier-Dokshitzer-Mueller-Peigné-Schiff and Zakharov (BDMPS-Z) formalism modified to consider emissions in the pre-hydrodynamics stage [71] was applied to extract the medium-induced radiation and revealed the importance of the early emissions. Recently, an analysis of the in-medium emission rate of soft gluons produced by jets showed the potential sensitivity of jets to the early-stage [72]. Using the Dynamical Radiative and Elastic Energy loss Approach (DREENA) [73–75], the effect of the early time dynamics was constrained by

R_{AA} and v_2 data for high- p_T and was shown to have a moderate contribution.

The presented literature shows the potential sensitivity of the hard probes on the pre-equilibrium stage. Nevertheless, in the glasma phase, most studies focus on the extraction of either momentum broadening or transport coefficients, which are not experimentally accessible quantities. Thus, the impact of the glasma stage on the dynamics of the hard probes is often implied indirectly. A series of exploratory works investigated the effect of glasma on heavy quark observables. Heavy quark spectra in an SU(2) glasma were extracted in both AA [35] and pA [33, 34] collisions. The resulting nuclear modification factor obtained in pA was shown to agree with the experimental D meson R_{pA} data. Furthermore, in AA it was reported that glasma dynamics generated an initial evolution of R_{AA} with a slope opposite to the standard heavy quark diffusion in the QGP [32]. Hence, it was suggested that this stage could yet be another mechanism contributing to the R_{AA} and v_2 puzzle, which was explored using mostly models applicable in the QGP stage [76–80]. However, since the glasma studies were done at a qualitative level, it still remains unclear what is the magnitude of the glasma effect. Hence, it is important to improve the previous models and continue investigating the impact of glasma on heavy quark spectra with additional model improvements.

The simultaneous description of R_{AA} and v_2 poses a challenge to existing theoretical models. It is considered that more differential observables, such as heavy flavor angular correlations [81], might offer better discrimination between various models. Additionally, the angular correlations are considered to be susceptible to the heavy quark production mechanism [82]. Inspired by this observation, one may question whether such an observable is potentially sensitive to the initial stage of the collision. Nevertheless, there is no current model calculation of heavy flavor angular correlations in the glasma. A related calculation done in the glasma is the evolution and dissociation of $Q\bar{Q}$ pairs studied in [40]. On the other hand, there are theoretical model estimates for the azimuthal correlations in the QGP. Heavy quark azimuthal angle correlations were extracted in [83] where the heavy quarks obey the Boltzmann equation with collisional and radiative energy loss effects, and evolve in an ideal hydrodynamic fluid whose initial condition is given by EPOS. Within a similar framework, the azimuthal correlations of heavy quark $Q\bar{Q}$ pairs were studied using EPOS4HQ, across multiple system sizes [84]. A simultaneous extraction of R_{AA} , v_2 and $c\bar{c}$ azimuthal correlations with Langevin dynamics was done in [85]. Results for the same observables were obtained using the Boltzmann equation with collisions [86]. However, these studies lack a treatment of the heavy quark dynamics in the pre-equilibrium stage. The potential sensitivity to the early dynamics motivates the investigation of azimuthal correlations for $Q\bar{Q}$ pairs in the evolving glasma.

The aim of this study is to investigate the impact of the

glasma stage on heavy quark observables, namely heavy flavor two-particle correlations and spectra. Throughout this work, we use our numerical solver for the classical transport of partons in the glasma background fields [50]. Firstly, we investigate correlations of heavy quarks evolving in the glasma. We start by initializing large ensembles of heavy quark and anti-quark pairs with opposite azimuthal angles and simulating their evolution in the glasma. Then, we evaluate their two-particle correlations in relative azimuthal angle $\Delta\phi$ and rapidity $\Delta\eta$ and extract the corresponding correlation widths $\sigma_{\Delta\phi}$ and $\sigma_{\Delta\eta}$. We study the time evolution of these correlation widths for charm and beauty quarks, along with the dependence on the glasma saturation momentum Q_s and heavy quark initial p_T . Secondly, we extract the nuclear modification factor R_{AA} in the glasma by studying how p_T momentum broadening in the glasma affects heavy quark p_T spectra. We perform numerical simulations of heavy quarks evolving in an SU(3) glasma, whose p_T distribution at formation time is given by the Fixed-Order+Next-to-Leading Logarithm (FONLL) heavy quark production calculation in pp , and extract R_{AA} . We study the proper time evolution, dependence on the glasma saturation momentum Q_s and initial collision energy \sqrt{s} , for charm and beauty quarks. Additionally, we improve our setup by initializing heavy quark p_T spectra with a FONLL calculation in AA which incorporates nuclear parton distribution function (nPDF) effects. Lastly, we compare the R_{AA} obtained from numerical glasma simulations with the prediction of an analytical toy model which assumes Gaussian p_T momentum kicks for any initial p_T .

This study begins with Sec. II which contains an overview of the theoretical framework and numerical implementation for the glasma fields and the classical transport of heavy quarks in these fields. In Sec. III, we outline our procedure to extract the two-particle correlations and the nuclear modification factor. The latter is evaluated from numerical simulations and using an analytical toy model for momentum broadening in glasma. Details about our choice for the numerical parameters and the obtained results are shown in Sec. IV, along with a detailed study of parameter dependencies. Lastly, in Sec. V we present concluding remarks and improvements planned for future studies. Additionally, Appendix A includes details about the classical color charge algebra of the SU(3) group and its effect on the extracted observables.

II. FRAMEWORK

In this section, we present the glasma framework and describe the numerical implementation for the evolution of the glasma fields. Additionally, this section contains an overview of the classical transport of probes in the glasma fields, along with our method to implement numerically the transport equations. More details are discussed in [50].

A. Glasma fields

The Color Glass Condensate effective theory [23–27] is based on a kinematic separation between the soft and hard partons within a high-energy nucleus. Since the nuclear wavefunction at high energies is mostly dominated by a large density of gluons [87], the soft fields have large occupation numbers and may be treated as classical. In this picture, the hard constituents, mostly valence quarks, are treated as a color current J^μ that generates the soft gauge fields A^μ representing the soft gluons. In this classical approximation, the coupled dynamics between the hard and soft sectors is encompassed in the classical Yang-Mills (CYM) equations

$$\mathcal{D}_\mu F^{\mu\nu} = J^\nu, \quad (1)$$

where $\mathcal{D}_\mu = \partial_\mu - ig[A_\mu, \cdot]$ is the covariant derivative, $F^{\mu\nu} = \partial_\mu A_\nu - \partial_\nu A_\mu - ig[A_\mu, A_\nu]$ the field strength tensor and g the coupling constant. Within the CGC framework, the color current J^μ generated by the hard partons is approximated using high energy kinematics and a classical probability distribution of color charges. More precisely, one assumes that the charges within nuclei which move along one of the light cone directions¹ x^\pm produce a current

$$J_{A,B}^{\mu,a}(x) = \delta^{\mu\pm} \delta(x^\mp) \rho_{A,B}^a(\vec{x}_\perp), \quad (2)$$

where a denotes the color index and ρ^a are classical color charge densities. One needs additional considerations to describe how classical color charge is distributed within the nucleus. For this purpose, we employ the McLerran-Venugopalan (MV) model [88–90], which is applicable for large nuclei with infinite transverse extent. Inside such nuclei, the color charges are assumed to be Gaussian stochastic variables which obey color neutrality and are uncorrelated in both color and transverse coordinates

$$\begin{aligned} \langle \rho_{A,B}^a(\vec{x}_\perp) \rangle &= 0, \\ \langle \rho_{A,B}^a(\vec{x}_\perp) \rho_{A,B}^b(\vec{y}_\perp) \rangle &= \delta^{ab} \delta^{(2)}(\vec{x}_\perp - \vec{y}_\perp) g^2 \mu_{A,B}^2. \end{aligned} \quad (3)$$

The MV model parameter $g^2\mu$ is the only physical variable in this ansatz and represents the color charge density inside each nucleus. One can show that $g^2\mu = \mathcal{O}(Q_s)$, where Q_s is the gluon saturation momentum and is approximately dictated by the collision energy. In numerical glasma simulations which implement the MV model, the proportionality factor between $g^2\mu$ and Q_s depends on the choice of the numerical parameters [91, 92]. The CYM field equations from Eq. (1) sourced by the light cone color current from Eq. (2) yield an analytic solution for the classical gauge field produced by a single CGC

¹ In our convention, the light cone coordinates are defined as $x^\pm \equiv (x^0 \pm x^3)/\sqrt{2}$, while $\vec{x}_\perp \equiv (x^1, x^2)$.

nucleus. In the light cone gauge this solution is given by transverse pure gauge field configurations [28, 29, 93]

$$\alpha_{A,B}^i(\vec{x}_\perp) = \frac{i}{g} V_{A,B}(\vec{x}_\perp) \partial^i V_{A,B}^\dagger(\vec{x}_\perp), \quad (4)$$

with the Wilson lines $V_{A,B}$ computed using the initial MV model color charges.

We proceed to the collision of CGC nuclei whose gauge potentials satisfy Eq. (4). We follow the standard prescription for constructing the resulting glasma fields [27–30] which relies on the boost-invariant approximation. The glasma fields are parametrized in the Milne coordinates, using the Milne proper time $\tau \equiv \sqrt{2x^+x^-}$ and the space-time rapidity $\eta_s \equiv \ln(x^+/x^-)/2$. In this coordinate system, the boost-invariance is imposed as an η_s -independence of the gauge fields, namely $A^\mu(x) = A^\mu(\tau, \vec{x}_\perp)$. Additionally, the glasma collision problem is formulated in the technically advantageous temporal gauge $A^\tau = 0$. The remaining gauge components are parametrized using the ansatz

$$\begin{aligned} A_C^i(\tau, \vec{x}_\perp) &= \theta_A \alpha_A^i(\vec{x}_\perp) + \theta_B \alpha_B^i(\vec{x}_\perp) + \theta_C \alpha_C^i(\tau, \vec{x}_\perp), \\ A_C^\eta(\tau, \vec{x}_\perp) &= \theta_C \alpha_C^\eta(\tau, \vec{x}_\perp), \end{aligned} \quad (5)$$

with the Heaviside functions $\theta_A \equiv \theta(-x^+) \theta(x^-)$, $\theta_B \equiv \theta(x^+) \theta(-x^-)$ for the light cone domain of the pure gauges generated by nuclei A, B , see Eq. (4), and $\theta_C \equiv \theta(x^+) \theta(x^-)$ for the forward light cone where the glasma fields reside. The theta functions assure the correct domains for the gauge fields of each of the colliding nuclei $\alpha_{A,B}$ and the resulting glasma $\alpha_C^{i,\eta}$ field in the forward light cone. Along the light cone, at $\tau \rightarrow 0^+$, the glasma initial condition satisfies the CYM equation of motion

$$\mathcal{D}_\mu F_C^{\mu\nu} \Big|_{\tau \rightarrow 0^+} = J_C^\nu, \quad \text{with} \quad J_C^\mu = J_A^\mu + J_B^\mu, \quad (6)$$

where $J_{A,B}^\mu$ are given by Eq. (2). The ansatz from Eq. (5) together with the CYM equation of motion (6) evaluated along the boundary of the light cone provide the initial condition

$$\begin{aligned} \alpha_C^i(\tau, \vec{x}_\perp) \Big|_{\tau \rightarrow 0^+} &= \alpha_A^i(\vec{x}_\perp) + \alpha_B^i(\vec{x}_\perp), \\ \alpha_C^\eta(\tau, \vec{x}_\perp) \Big|_{\tau \rightarrow 0^+} &= \frac{ig}{2} [\alpha_A^i(\vec{x}_\perp), \alpha_B^i(\vec{x}_\perp)], \end{aligned} \quad (7)$$

expressible solely from the pure gauge fields given in Eq. (4). The corresponding initial glasma chromo-electromagnetic fields are purely longitudinal [29, 94, 95].

The expressions from Eq. (7) are used to initialize the glasma fields at $\tau \rightarrow 0^+$. The proper time evolution at $\tau > 0$ is then given by the sourceless CYM equations. In Milne coordinates, the field equations read [28, 96]

$$\begin{aligned} \frac{1}{\tau^3} \partial_\tau \tau^3 \partial_\tau \alpha^\eta - [\mathcal{D}^i, [\mathcal{D}^i, \alpha^\eta]] &= 0, \\ \frac{1}{\tau} [\mathcal{D}^i, \partial_\tau \alpha^i] - ig\tau [\alpha^\eta, \partial_\tau \alpha^\eta] &= 0, \quad (8) \\ \frac{1}{\tau} \partial_\tau \tau \partial_\tau \alpha^i - ig\tau^2 [\alpha^\eta, [\mathcal{D}^i, \alpha^\eta]] - [\mathcal{D}^j, F^{ji}] &= 0, \end{aligned}$$

and can be further solved numerically.

To assure a numerically gauge invariant discretization, we use a real-time lattice gauge theory formulation of these equations [97–99]. Due to boost-invariance, α^η behaves as a scalar under the η_s -independent non-Abelian gauge transformation. The transverse gauge fields α^i are replaced by gauge links, which represent the shortest Wilson lines on the lattice²

$$\alpha^i(\tau, \vec{x}_\perp) \xrightarrow{\text{lattice}} U_{\mathbf{x},\hat{i}}(\tau) \approx \exp \left\{ ig a \alpha^i \left(\tau, \vec{x}_\perp + \frac{a}{2} \hat{i} \right) \right\}. \quad (9)$$

Similarly, the corresponding field strength tensor F^{ij} is represented by a plaquette variable, which constitutes the simplest Wilson loop constructed on the lattice

$$\begin{aligned} F^{ij}(\tau, \vec{x}_\perp) \xrightarrow{\text{lattice}} U_{\mathbf{x},\hat{i}\hat{j}}(\tau) \\ \approx \exp \left\{ ig a^2 F^{ij} \left(\tau, \vec{x}_\perp + \frac{a}{2} \hat{i} + \frac{a}{2} \hat{j} \right) \right\}. \end{aligned} \quad (10)$$

The CYM evolution for the glasma fields from Eqs. (8) is recast as a set of partial differential equations for the proper time τ evolution of $\alpha_{\mathbf{x}}^\eta(\tau)$, $U_{\mathbf{x},\hat{i}}(\tau)$, and $U_{\mathbf{x},\hat{i}\hat{j}}(\tau)$ in each lattice site \mathbf{x} . We solve these numerically using the leapfrog method [97–99] implemented in the curraun solver³. More technical details on the lattice discretization and numerical implementation of this solver are provided in [50, 100].

B. Test particles

The classical transport of probes in a Yang-Mills background field is described by Wong's equations [101, 102]. In Milne coordinates, they are expressible as

$$\frac{dx^\mu}{d\tau} = \frac{p^\mu}{p^\tau}, \quad (11a)$$

$$\frac{Dp^\mu}{d\tau} = \frac{g}{T_R} \text{Tr} [Q F^{\mu\nu}] \frac{p_\nu}{p^\tau}, \quad (11b)$$

$$\frac{dQ}{d\tau} = -ig [A_\mu, Q] \frac{p^\mu}{p^\tau}, \quad (11c)$$

where $(p^\tau)^2 \equiv (p^x)^2 + (p^y)^2 + \tau^2 (p^\eta)^2 + m^2$, m is the test particle mass, $D/d\tau$ denotes the covariant derivative in curvilinear coordinates and T_R is the coefficient in $\text{Tr} [T^a T^b] = T_R \delta^{ab}$. Wong's equations represent the equations of motion for classical test particles probing a Boltzmann-Vlasov distribution function [103–106]. By solving Wong's equations, we effectively sample the distribution function of a collisionless Vlasov kinetic plasma.

² Here $a = L/N$ is the lattice spacing of a square transverse lattice with length L and $N \times N$ lattice sites, $\mathbf{x} \equiv (x_i, y_i)$ is the transverse coordinate of a lattice site $i \in \{1, \dots, N\}$ and \hat{i} is the unit vector along $i \in x, y$.

³ Publicly available at github.com/openpixi/curraun.

There is no energy loss mechanism included in this formalism, neither by collisions with other particles nor from classical bremsstrahlung. The momentum evolution from Eq. (11b) is driven by the color Lorentz force in curvilinear coordinates $\mathcal{F}_\mu \equiv F_{\mu\nu}p^\nu/p^\tau$. Thus, the classical particles experience momentum deflections due to the background chromo-electromagnetic fields. The classical color charge evolution from Eq. (11c) may be recast as a color rotation⁴

$$Q(\tau) = \mathcal{U}^\dagger(\tau_0, \tau) Q(\tau_0) \mathcal{U}(\tau_0, \tau), \quad (12)$$

where the particle Wilson line accumulates the background gauge field along its trajectory as

$$\mathcal{U}^\dagger(\tau_0, \tau) = \mathcal{P} \exp \left(-ig \int_{x^\mu(\tau_0)}^{x^\mu(\tau)} dx^\mu A_\mu(x^\mu(\tau)) \right). \quad (13)$$

The color charges are chosen as elements of the classical Lie algebra $\mathfrak{su}(3)$. The equations of motion conserve the values of the classical quadratic $q_2(R)$ and cubic $q_3(R)$ Casimirs⁵

$$Q^a Q^a \equiv q_2(R), \quad d_{abc} Q^a Q^b Q^c \equiv q_3(R), \quad (14)$$

in the representation R . Here, Q^a are the (representation-dependent) color components of the color charge $Q = Q^a T^a$. We are mainly interested in the fundamental $R = F$ representation for quarks. We generate random initial color charges $Q(\tau_0)$ with fixed values for $q_{2,3}$, which then remain conserved under color rotations according to Eq. (12).

We simulate point particles at continuous spatial coordinates (\vec{x}_\perp, η_s) according to the coordinate evolution, Eq. (11a), in a gauge field that is discretized on a lattice in the transverse coordinate. The equation for the Lorentz force, Eq. (11b), thus requires associating a discrete lattice point to a continuous coordinate. For this we use the nearest grid point (NGP) approximation $\vec{x}_\perp(\tau_n) \approx \text{NGP}(\vec{x}_\perp(\tau_n)) = \mathbf{x}_n$ which replaces the particle transverse coordinates with the closest lattice site $\mathbf{x}_n \equiv \mathbf{x}(\tau_n)$. No approximations are required for the $\eta_s(\tau_n)$ rapidity coordinate. The particle Wilson line from Eq. (13) is numerically approximated as a product of infinitesimal timesteps as $\mathcal{U}(\tau_0, \tau_m) = \prod_n \mathcal{U}(\tau_{n-1}, \tau_n)$, with $n \in \{1, m\}$. Each of the infinitesimal Wilson lines involved in the product simplifies to a product of Wilson lines in the different coordinate directions

$$\begin{aligned} \mathcal{U}(\tau_{n-1}, \tau_n) &\simeq \exp \left(ig \int_{\mathbf{x}_{n-1}}^{\mathbf{x}_n} dy^i A_i(\mathbf{y}) \right) \\ &\times \exp(ig\delta\eta_n A_\eta(\mathbf{x}_n)) = U_{\mathbf{x}_{n-1}, \hat{i}}(\tau_n) U_{\mathbf{x}_n, \hat{\eta}}(\tau_n). \end{aligned} \quad (15)$$

⁴ Inspired by the Colored Particle-in-Cell (CPIC) method for classical simulations of particles in non-Abelian fields [107–111].

⁵ Defined in analogy with the group theory Casimir invariants [112] $T^a T^a \equiv C_2(R) \mathcal{I}_R$ and $d_{abc} T^a T^b T^c \equiv C_3(R) \mathcal{I}_R$, where \mathcal{I} is the identity matrix in the given representation R .

The infinitesimal particle color charge rotation is performed using the transverse gauge link variables $U_{\mathbf{x}, \hat{i}}$ and a rapidity gauge link $U_{\mathbf{x}, \hat{\eta}}$ constructed from $A_{\mathbf{x}, \eta}$. This method of discretizing the color rotations has the advantage that, by construction, $Q \in \mathfrak{su}(N_c)$ throughout the evolution and the Casimir invariants from Eq. (14) are numerically conserved for any $Q(\tau)$. We use the following method to randomly generate classical color charges with desired values for the Casimir invariants in Eq. (14). We start from a handpicked initial Q_0 which satisfies the Casimir constraints $q_{2,3}(Q_0)$ and randomize it by performing random $U \in \text{SU}(N_c)$ rotations as $Q(\tau_0) = U Q_0 U^\dagger$. This initial charge is used as input in Eq. (12) and is then rotated at each time step with the numerical particle Wilson line from Eq. (15). Using these procedures, we perform numerical color rotations in an $\text{SU}(3)$ gauge invariant manner.

These features are incorporated in our numerical solver for Wong's equations in the glasma background fields⁶, which was developed and tested in our previous work [50].

III. COMPUTING OBSERVABLES

This section outlines the techniques used to calculate the two-particle correlations and the nuclear modification factor for heavy quarks as they evolve in the glasma. We explain the procedure to compute the correlation width of $Q\bar{Q}$ pairs from the two-particle correlation and describe how heavy quark p_T spectra are extracted using either our numerical solver or an analytical toy model.

A. Two-particle correlations

We simulate the transport of heavy quark Q and anti-quark \bar{Q} pairs in the evolving glasma, initially produced back-to-back in azimuthal angle, as suggested by leading order (LO) pQCD heavy quark production [18, 113]. At next-to-leading order (NLO), the $Q\bar{Q}$ pairs are no longer formed back-to-back [114, 115]. However, this being the first study of $Q\bar{Q}$ angular correlations, we consider the back-to-back case to have a more direct understanding of the decorrelation induced by the glasma dynamics. The coordinates, momenta, and color charges of the quarks in the pair are initialized according to simple toy models. Each heavy quark of mass m has a fixed initial transverse momentum $p_T(\tau_{\text{form}})$ and is formed at a proper time given by $\tau_{\text{form}} = 1/(2m_T)$, where the transverse mass is $m_T^2 = m^2 + p_T^2(\tau_{\text{form}})$. The quark and anti-quark have opposing momenta with the same magnitude, namely $\vec{p}_T^Q(\tau_{\text{form}}) = -\vec{p}_T^{\bar{Q}}(\tau_{\text{form}})$, where $\vec{p}_T \equiv (p^x, p^y)$. In all our particle simulations $p^\eta(\tau_{\text{form}}) = 0$. The quarks in the pair are produced at the same position. Their

⁶ Available at github.com/avramescudana/curraun/tree/wong.

coordinates $x_T(\tau_{\text{form}})$ are randomly distributed in the transverse simulation region, where $x_T \equiv (x, y)$, while $\eta(\tau_{\text{form}}) = 0$. In the following, we denote by N_{tp} the number of test particles in the evolution. The $Q\bar{Q}$ pair is not necessarily color neutral since the main mechanism of heavy quark pair production is via gluon fusion $gg \mapsto Q\bar{Q}$. Additionally, the color charges suffer multiple color rotations in the glasma and are very rapidly decorrelated from their initial charges. Thus we treat the initial classical color charges of the Q and \bar{Q} as being random and independent of each other. However, one should not expect an effect from the specific initial color distribution due to the fast stochastic color charge evolution.

We evolve the $Q\bar{Q}$ pair in the glasma background fields using our numerical solver. Wong's equations for coordinates and momenta (11b) in Milne coordinates provide (x, y, η_s) and (p^x, p^y, p^η) for both the Q and \bar{Q} at each proper time τ . We further extract the laboratory frame longitudinal momentum $p^z = \sinh \eta_s p^\tau + \cosh \eta_s \tau p^\eta$, where $(p^\tau)^2 = p_T^2 + (\tau p^\eta)^2 + m^2$ and $p_T^2 = (p^x)^2 + (p^y)^2$, along with the pseudorapidity of each quark in the pair as

$$\eta^q \equiv \frac{1}{2} \ln \frac{p^q + p_z^q}{p^q - p_z^q}, \quad \text{where } q \in \{Q, \bar{Q}\}, \quad (16)$$

with $(p^q)^2 = (p_T^q)^2 + (p_z^q)^2$ for $q \in \{Q, \bar{Q}\}$. The relative pseudorapidity is given by

$$\Delta\eta \equiv \eta^Q - \eta^{\bar{Q}}. \quad (17)$$

We compute the relative azimuthal angle between the quark pair using the scalar and vector product of the transverse momenta of the quarks as

$$\Delta\phi \equiv \arctan \left(\frac{\vec{p}_T^Q \times \vec{p}_T^{\bar{Q}} \cdot \vec{n}}{\vec{p}_T^Q \cdot \vec{p}_T^{\bar{Q}}} \right), \quad (18)$$

where \vec{n} is an arbitrary two-dimensional unit vector with $|\vec{n}| = 1$. A sketch showing the evolution and extraction of $\Delta\phi$ and $\Delta\eta$ for a $Q\bar{Q}$ pair overlaid on the glasma energy density profile from a numerical simulation is depicted in Fig. 1.

After simulating large ensembles of test particles N_{tp} in a single glasma event, and a sufficiently large number of glasma events N_{events} , we collect all the $(\Delta\eta_i, \Delta\phi_i)$ where $i \in \{1, \dots, N_{\text{tp}} \times N_{\text{events}}\}$. Then, we extract the two-particle correlations

$$\mathcal{C}(\Delta\eta, \Delta\phi) \equiv \frac{1}{N_{\text{pairs}}} \frac{d^2 N}{d\Delta\eta d\Delta\phi}, \quad (19)$$

and study them as a function of the relative proper time $\Delta\tau \equiv \tau - \tau_{\text{form}}$, to account for the finite formation time of the quarks in the pair. In practice, we extract these correlations using Kernel Density Estimators (KDEs)⁷. By

integrating Eq. (19) along $\Delta\eta$ or $\Delta\phi$ we also extract the azimuthal and pseudorapidity correlations

$$\mathcal{C}(\Delta\phi) \equiv \frac{1}{N_{\text{pairs}}} \frac{dN}{d\Delta\phi}, \quad \mathcal{C}(\Delta\eta) \equiv \frac{1}{N_{\text{pairs}}} \frac{dN}{d\Delta\eta} \quad (20)$$

as a function of $\Delta\tau$. The momentum kicks in the glasma cause the initial correlation to get smeared out, yielding a symmetric roughly Gaussian distribution in both $\Delta\eta$ and $\Delta\phi$. This is schematically represented in Fig. 2. To quantify the degree of decorrelation for the initial $Q\bar{Q}$ pair after evolving in the glasma, we further evaluate the $\Delta\tau$ evolution for the widths $\sigma_{\Delta\eta}$ and $\sigma_{\Delta\phi}$ of the correlations $\mathcal{C}(\Delta\eta)$ and $\mathcal{C}(\Delta\phi)$ defined in Eq. (20). In practice, we extract the widths $\sigma_{\Delta\eta}$ and $\sigma_{\Delta\phi}$ using the standard deviation of the distributions $\mathcal{C}(\Delta\eta)$ and $\mathcal{C}(\Delta\phi)$.

B. Nuclear modification factor

Classical particles evolving in the glasma experience momentum deflections due to the background electromagnetic fields. The convolution of the probability distribution of deflections with the initial spectrum of quarks leads to a modification of the final p_T -spectrum from the initial one. This modification is often quantified by a ratio of the final and initial p_T spectra. We rely on heavy quark production pQCD calculations [113, 116–119] to initialize a realistic initial p_T -spectrum. We use the FONLL (Fixed Order + Next-to-Leading Logarithm) [117, 120] heavy quark differential cross section $d\sigma/dp_T$ to distribute the initial probability $dN/dp_T(\tau_{\text{form}})$ at the formation time of the quark. We study only bare quarks and no fragmentation functions to the subsequent mesons are considered. The FONLL calculation is used to initialize heavy quark spectra with both proton and nuclear parton distribution functions (PDFs and nPDFs), at different center-of-mass collision energies \sqrt{s} . We denote the choice of the PDF by a superscript “pp” or “AA” in the following. Moreover, each FONLL heavy quark production cross section comes with factorization and renormalization scales, heavy quark mass and PDF uncertainties. In practice, we approximate the FONLL distribution with a fit performed on a logarithmic scale, which lies within the aforementioned uncertainties

$$\frac{d\sigma^{pp/AA}}{dp_T}(\sqrt{s}, \text{PDF/nPDF}) = \frac{x_0 p_T}{(1 + x_3 p_T^{x_1})^{x_2}}. \quad (21)$$

Here the fit parameters (x_0, x_1, x_2, x_3) depend on the initial \sqrt{s} , PDF choice for pp or nPDF choice for AA collisions, and quark flavor. Our choices for PDFs are CTEQ6.6 [121] and the combination CT14NLO [122] for PDF and EPPS16 [123] for nPDF. We use the FONLL p_T differential cross section, normalized by the total p_T integrated cross section, to construct the probability dis-

⁷ Package `KernelDensity.jl` implemented in Julia.

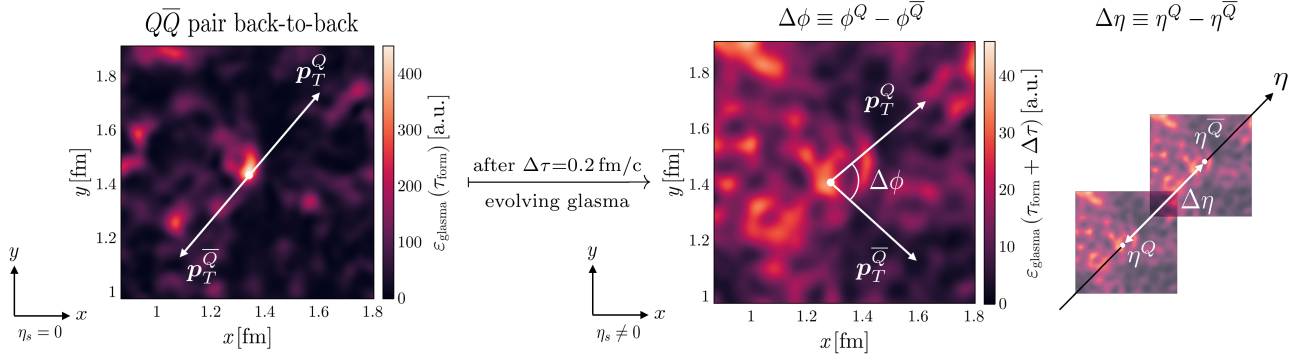


FIG. 1. Schematic representation of a single quark (Q) anti-quark (\bar{Q}) pair evolving in the glasma background field. The quarks in the pair are initialized with opposite $\mathbf{p}_T^Q = -\mathbf{p}_T^{\bar{Q}}$, where $\mathbf{p}_T \equiv (p^x, p^y)$. The background depicts a boost invariant slice of the glasma energy density at the formation time of the quarks $\varepsilon(\tau_{\text{form}})$. After $\Delta\tau$, as the quarks in the pair get deflected by the evolving glasma, their relative azimuthal angle $\Delta\phi \equiv \phi^Q - \phi^{\bar{Q}}$ and pseudorapidity $\Delta\eta \equiv \eta^Q - \eta^{\bar{Q}}$ shift from the initial peak at $\Delta\phi(\tau_{\text{form}}) = \pi$ and $\Delta\eta(\tau_{\text{form}}) = 0$. After $\Delta\tau$, the transverse coordinates of the quarks change are still depicted at the same position even though they numerically change.

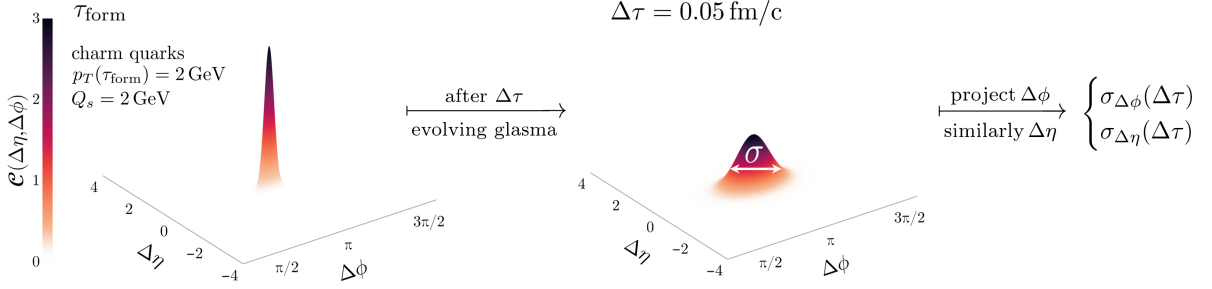


FIG. 2. Sketch of the azimuthal and rapidity decorrelation of $Q\bar{Q}$ pairs evolving in the glasma, along with the proper time evolution of the decorrelation widths in $\Delta\phi$ and $\Delta\eta$. The initial two-particle correlation is peaked at $\mathcal{C}(\Delta\phi, \Delta\eta) \propto \delta(\Delta\phi - \pi)\delta(\Delta\eta)$ but after $\Delta\tau$ it gets washed out by the glasma. This is quantified through the decorrelation widths $\sigma_{\Delta\phi}$ and $\sigma_{\Delta\eta}$ of the projected two-particle correlations along $\Delta\phi$ and $\Delta\eta$ respectively, extracted at different proper time values $\Delta\tau$.

tribution of heavy quarks produced at τ_{form} in the glasma

$$\frac{dN^{pp/AA}}{dp_T}(\tau_{\text{form}}) = \frac{1}{\sigma_{\text{tot}, Q\bar{Q}}^{pp/AA}} \frac{d\sigma_{Q\bar{Q}}^{pp/AA}}{dp_T}, \quad (22)$$

where A is the nuclear mass number and $\sigma_{\text{tot}, Q\bar{Q}} = \int dp_T d\sigma_{Q\bar{Q}}/dp_T$ represents the total $Q\bar{Q}$ cross section but for simplicity we further denote it as σ_{tot} . The dependence of the quark probability density on \sqrt{s} and PDF in pp or nPDF in AA is implicit. Note that throughout this work dN/dp_T refers to the probability distribution and not multiplicity, i.e. $\int dp_T dN/dp_T = 1$.

The heavy quark test particles, distributed according to the initial p_T spectrum at formation time $dN/dp_T(\tau_{\text{form}})$ in Eq. (22) from the FONLL fit in Eq. (21), evolve in the glasma fields and experience p_T momentum broadening. The resulting probability distribution $dN/dp_T(\tau)$ in the glasma depends on the evolution time τ . The change in the p_T distribution due to

the glasma is encoded in the nuclear modification factor defined as

$$R_{AA}(\tau) = \frac{1}{A^2} \frac{\sigma_{\text{tot}}^{AA}}{\sigma_{\text{tot}}^{pp}} \frac{dN}{dp_T}(\tau; pp/AA) \frac{dN^{pp}}{dp_T}(\tau_{\text{form}}). \quad (23)$$

Recall that the notation pp/AA used in the glasma spectrum refers to the input FONLL calculation used to initialize the heavy quark distribution from Eq. (22), namely pp with a specified PDF or AA with an nPDF. When a pp FONLL initialization is used, the total cross section is simply $\sigma_{\text{tot}}^{AA} = A^2 \sigma_{\text{tot}}^{pp}$ and the nuclear modification factor R_{AA} from Eq. (23) becomes the ratio of the (normalized) probability distributions for heavy quarks before and after evolving in the glasma. Thus, in this case, R_{AA} must obey a ‘‘sum rule’’ where values $R_{AA} > 1$ must be compensated by $R_{AA} < 1$ at another p_T . For the AA FONLL input calculation, due to nuclear PDF effects, $\sigma_{\text{tot}}^{AA} < A^2 \sigma_{\text{tot}}^{pp}$ and consequently $R_{AA} < 1$ even

without any effects from the glasma.

In practice, to evaluate R_{AA} from Eq. (23), we extract heavy quark spectra after their evolution in the glasma phase directly from numerical simulations. We will compare these to the toy model discussed below which assumes Gaussian broadenings at fixed p_T .

1. Numerical R_{AA} (glasma simulations)

Similarly to the initialization for the $Q\bar{Q}$ pairs in Sec. III A, we simulate heavy quark test particles with given mass m , initial $p_T(\tau_{\text{form}})$ whose evolution in the glasma starts at $\tau_{\text{form}} = 1/(2m)$. The quarks are randomly distributed uniformly in transverse coordinate $x_T(\tau_{\text{form}})$. We initialize the transverse momenta p_T for ensembles of N_{tp} test particles according to the FONLL spectra for either pp or AA collisions from Eq. (21). At fixed τ values, the distribution of the quarks is numerically reconstructed, $dN/dp_T(\tau)$ is extracted as a KDE and R_{AA} is computed using Eq. (23). This procedure is repeated for many glasma events N_{events} . In practice, the sampling from the FONLL spectra is implemented using a weighting procedure. More precisely, we perform the evolution in the glasma of a large ensemble of test particles initialized according to a flat p_T -distribution and construct $dN/dp_T(\tau)$ as a weighted KDE, where the weights are given by the initial $dN/dp_T(\tau_{\text{form}})$ for each p_T value. Compared to a straightforward sampling from the steeply falling FONLL spectrum this reweighting procedure reduces the number of glasma events required to obtain enough statistics at high p_T . We have also checked this reweighting method with a direct sampling from the FONLL distribution. This weighting procedure is schematically depicted in Fig. 3.

2. Analytical R_{AA} (toy model)

In addition to the full glasma simulation, we also study a simple toy model for the glasma modification of the single quark spectrum. For this purpose, we assume that the momentum accumulation obeys a two-dimensional Gaussian in (p_x, p_y) as represented in Fig. 4. The width of the Gaussian can then be taken to depend on the proper time $\Delta\tau$. Thus, the heavy quarks acquire transverse p_T momentum kicks, causing their p_T distribution to change. The effect of such Gaussian momentum kicks on the probability distribution dN/dp_T is depicted in Fig. 4 for charm quarks initialized with a selection of values for $p_T(\tau_{\text{form}})$.

Let us denote the p_T distribution of quarks in the glasma at a certain proper time τ value as

$$\mathcal{N}_\tau(p_T) \equiv \frac{dN}{dp_T}(p_T, \tau), \quad (24)$$

with $\mathcal{N}_0 \equiv \mathcal{N}_{\tau_{\text{form}}}$ the initial distribution, chosen according to Eq. (21) for the pp case. Using this notation, the

nuclear modification factor defined in Eq. (23) is, in the absence of nPDF effects, expressed as

$$R_{AA}(p_T, \tau; \mathcal{N}_0) = \frac{\mathcal{N}_\tau(p_T)}{\mathcal{N}_0(p_T)} \quad (25)$$

and \mathcal{N}_τ implicitly depends on the initial distribution \mathcal{N}_0 .

In the Gaussian toy model, we assume that the broadening of particle momentum, initialized as $p_T(\tau_0)$, is described by a Gaussian. Moreover, we assume that each p_T -bin is affected independently, which corresponds to the fact that there are no interactions and thus no momentum exchange between particles. For a given initial $\vec{q} \equiv (q_x, q_y)$, the momentum exchange is symmetrically centered around the initial momentum \vec{q} and has the same widths $\sigma_x = \sigma_y \equiv \sigma$ along the transverse directions

$$\mathcal{K}_\tau(\vec{q}, \vec{p}) = \frac{1}{2\pi\sigma_\tau^2(q_T)} \exp\left\{-\frac{(\vec{p}-\vec{q})^2}{2\sigma_\tau^2(q_T)}\right\}. \quad (26)$$

The width of the Gaussian could be taken to be a function of the initial transverse momentum $q_T \equiv \sqrt{q_x^2 + q_y^2}$ and the proper time τ , although for simplicity, we assume that it is independent of the initial p_T . Different values of the glasma saturation momentum Q_s and the particle quadratic Casimir q_2 can be modeled by different values for the width.

The spectrum at τ is a convolution of the initial spectrum \mathcal{N}_0 with all possible Gaussian p_T -migrations from Eq. (26), namely

$$\mathcal{N}_\tau(p_T) = \int d\theta_p \iint d^2\vec{q} \mathcal{K}_\tau(\vec{q}, \vec{p}) \mathcal{N}_0(q_T) \quad (27)$$

where $\theta_p \equiv \arctan(p_x/p_y)$. After expressing Eq. (27) in polar coordinates and using the integral representation of the modified Bessel function of the first kind I_0 [124], the evolved spectrum \mathcal{N}_τ used to extract the nuclear modification factor from Eq. (25) becomes

$$\mathcal{N}_\tau(p_T; \mathcal{N}_0) = \int dq_T \frac{\pi q_T}{2\sigma_\tau^2(q_T)} \times \exp\left\{-\frac{p_T^2 + q_T^2}{2\sigma_\tau^2(q_T)}\right\} \mathcal{N}_0(q_T) I_0\left(\frac{p_T q_T}{\sigma_\tau^2(q_T)}\right). \quad (28)$$

Once the width $\sigma_\tau(q_T)$ is fixed and the initial distribution \mathcal{N}_0 is known, in our case from the FONLL calculation in Eq. (21), the integral from Eq. (28) may be performed numerically. The resulting toy model R_{AA} encodes the approximation of perfectly Gaussian momentum broadening in the glasma.

IV. RESULTS

This section contains an overview of the numerical parameters used as input in our numerical solver, to initialize the glasma fields and the heavy quark transport in

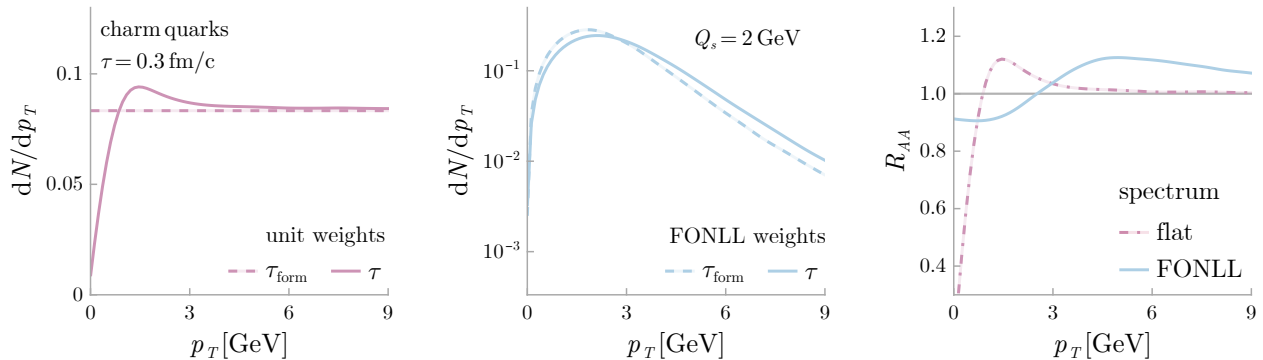


FIG. 3. Heavy quark p_T spectra (*left and middle*) and their corresponding nuclear modification factor R_{AA} (*right*). The *left subfigure* depicts the effect of the glasma at τ on an initially flat- p_T distribution at τ_{form} , while the *middle subfigure* contains the glasma spectra weighted by the initial FONLL distribution.

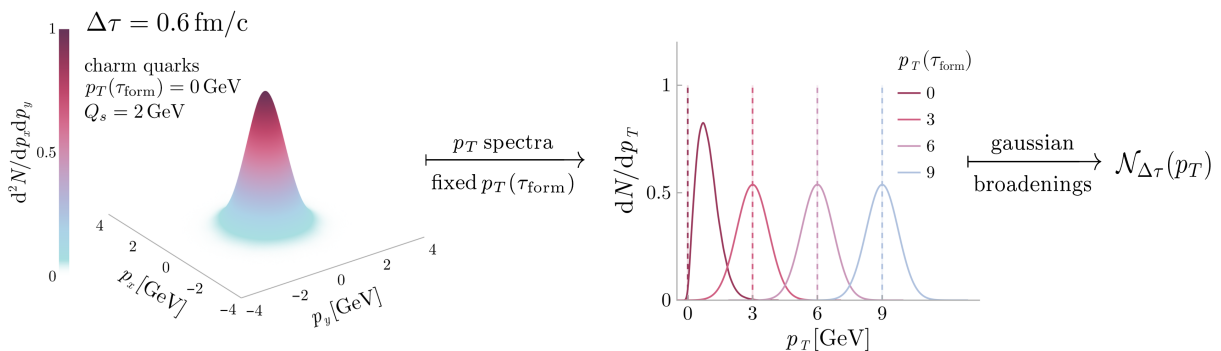


FIG. 4. Broadening in (p_x, p_y) at a fixed $\Delta\tau$ for charm quarks initialized with a given $p_T(\tau_{\text{form}})$, with various values of initial $p_T(\tau_{\text{form}}) \in \{0, 3, 6, 9\}$ GeV. In our Gaussian toy model introduced in Sec. III B 2, we approximate this p_T -broadening by a Gaussian, which leads to the expression in Eq. (28) for the modified momentum distribution.

these fields. Further, we provide more numerical details about our procedure to extract the two-particle correlations of $Q\bar{Q}$ pairs and the heavy quark nuclear modification factor R_{AA} , following their evolution in the glasma, and showcase the key findings.

A. Numerical parameters

We simulate glasma fields obtained in collisions at LHC between lead nuclei, where the value of the saturation momentum in central events roughly corresponds to $Q_s = 2$ GeV. Since the choice of Q_s is slightly ambiguous, we study the dependence on the initial Q_s of our observables of interest. The relation with the MV model parameter from Eq. (3) is given by $g^2\mu \approx 0.8Q_s$. In classical Yang-Mills theory, the coupling constant $g^2 = 4\pi\alpha_s(Q_s)$ can be scaled out from the equations of motion, but the explicit value is needed in order to express quantities such as the energy density into physical units. Its value is taken to run in accordance with the saturation momen-

tum as

$$\alpha_s(Q_s) = \frac{1}{33 - 3N_f \ln \frac{Q_s^2}{\Lambda_{\text{QCD}}^2}}, \quad (29)$$

where $N_f = 3$ and $\Lambda_{\text{QCD}} = 200$ MeV. The most important numerical parameters of the lattice are the transverse simulation length which we take to be $L = 10$ fm and the number of lattice points $N = 512$.

The heavy quark test particles are distributed uniformly in the transverse simulation region $\vec{x}_\perp(\tau_{\text{form}}) \in [0, L]^2$, while their initial space-time rapidity is null $\eta_s(\tau_{\text{form}}) = 0$. Each heavy quark is given an initial transverse momentum $p_T(\tau_{\text{form}})$ and is formed at a fixed initial τ_{form} equal to the inverse of its mass. We study charm and beauty quarks with given masses $m_c = 1.27$ GeV and $m_b = 4.18$ GeV [125]. Typically, we use a single glasma event for $N_{\text{tp}} = 10^5$ such heavy quark test particles. We simulate multiple glasma events with variable N_{events} , until convergence for our chosen quantity is numerically achieved.

Numerically, we sample the color charge components of the heavy quarks such that they satisfy the Casimir

constraints from Eq. (14) with $q_2 = C_2(F)$ and $q_3 = 0$, where $C_2(F) = 4/3$ is the SU(3) group theory Casimir in the fundamental representation. More details are provided in Appendix A 1. This choice is based on our previous observation [50] that the momentum broadening for partons in certain kinematic scenarios, such as eikonal jets and static quarks, scales with the quadratic Casimir $\langle p^2 \rangle_R \propto q_2(R)$ and is independent of the cubic one $q_3(R)$. Inspired by this observation, we numerically check that this scaling holds for $\langle p^2 \rangle$ of heavy quarks beyond the infinite mass approximation, with the corresponding change in the width of the azimuthal $\sigma_{\Delta\phi}$ and rapidity correlations $\sigma_{\Delta\eta}$. The results are shown in Appendix A 2. In a similar way, we checked that the p_T -spectra of heavy quarks in the glasma are independent of q_3 .

B. Two-particle correlations

Based on the setup described in Sec. III A, we numerically extract the azimuthal and rapidity two-particle correlation $\mathcal{C}(\Delta\eta, \Delta\phi)$ using Eq. (19) for pairs of charm or beauty quarks and their corresponding antiquarks, throughout their evolution in the glasma. As shown in Fig. 5, the initial correlation is a peak $\mathcal{C}(\tau_{\text{form}}) \propto \delta(\Delta\phi - \pi)\delta(\Delta\eta)$, which quickly starts to decorrelate in $\Delta\eta$ at $\Delta\tau = 0.01$ fm/c, followed by a decorrelation in $\Delta\phi$ at $\Delta\tau = 0.1$ fm/c. Around the typical switching time to a kinetic theory followed by a hydrodynamics description [126] at $\Delta\tau = 0.2 - 0.3$ fm/c, most of the initial correlation gets significantly reduced. The results represented in Fig. 5 correspond to charm quarks with $p_T(\tau_{\text{form}}) = 1$ GeV as they propagate in a glasma characterized by $Q_s = 2$ GeV.

We first show in Fig. 6 the azimuthal angle decorrelation of charm quark pairs initialized with $p_T = 2$ GeV in the glasma. More concisely, we numerically extract $\mathcal{C}(\Delta\phi)$ as a function of $\Delta\phi$ at various values of the proper time $\Delta\tau$. The results represented in Fig. 6 show that the initial correlation $\mathcal{C}(\Delta\phi) \propto \delta(\Delta\phi - \pi)$ rapidly decreases until $\Delta\tau = 0.05$ fm/c, when the glasma fields are strong. This decrease becomes slower for $\Delta\tau > 0.1$ fm/c characterized by dilute fields. The rapidity correlation $\mathcal{C}(\Delta\eta)$ shows similar behaviour.

To systematically quantify the decorrelation in the glasma and to study the initial particle $p_T(\tau_{\text{form}})$ and glasma Q_s dependence of the correlation, we extract the rapidity $\sigma_{\Delta\eta}$ and azimuthal $\sigma_{\Delta\phi}$ decorrelation widths, as a function of the time passed from the formation of the quark $\Delta\tau$. The decorrelation widths are extracted from Eq. (20) and the procedure is depicted in Fig. 2. The dependence of the decorrelation widths $\sigma_{\Delta\phi}$ and $\sigma_{\Delta\eta}$ on the quark p_T at formation time τ_{form} is shown in Fig. 7 as a function of the relative proper time $\Delta\tau$, for both charm and beauty quarks. The longitudinal decorrelation $\sigma_{\Delta\eta}$ in rapidity is systematically greater than the azimuthal $\sigma_{\Delta\phi}$, which is extracted from the transverse momenta, as expressed in Eq. (18). Since the glasma ini-

tially consists of only longitudinal color fields, quantities affected by the longitudinal dynamics tend to be larger than the corresponding transverse ones. We reported a similar ordering in our previous work [50] for momentum broadening components $\langle \delta p_L^2 \rangle > \langle \delta p_T^2 \rangle$ and we interpret $\sigma_{\Delta\eta} > \sigma_{\Delta\phi}$ as arising from the same anisotropic glasma dynamics. As expected, the widths $\sigma_{\Delta\eta}$, $\sigma_{\Delta\phi}$ decrease with increasing p_T . This is natural since heavy quark pairs initialized with small p_T only require a small momentum transfer from the glasma fields to decorrelate, while pairs with sufficiently large p_T still preserve the initial correlation throughout the evolution. In realistic collisions, assuming heavy quarks produced according to the FONLL distribution from Eq. (21), most quarks have small initial p_T and thus one expects the glasma stage to completely decorrelate the bulk of $Q\bar{Q}$ pairs. However, it is experimentally possible to also access the angular correlation between particles at intermediate and high p_T values that do not completely lose their correlation, hence could carry novel and relevant information about the heavy quark in medium diffusion and energy loss.

Figure 8 shows a similar analysis for the Q_s dependence of $\sigma_{\Delta\phi}$ and $\sigma_{\Delta\eta}$, while keeping the initial momenta fixed to the moderate value $p_T(\tau_{\text{form}}) = 2$ GeV, for both charm and beauty quarks. The decorrelation widths in Fig. 8 are shown in terms of $Q_s\Delta\tau$, the dimensionless relevant temporal scale in the glasma. Although in general the saturation time of the glasma dynamics is considered to be $1/Q_s$, our quantitative study in SU(3) shows that the saturation of both the azimuthal and longitudinal widths occurs at $\tau \simeq 3/Q_s$. In the case of typical Q_s values for AA collisions, this implies $\tau \simeq 0.3$ fm/c, which is in good agreement with the typical initial time of the hydrodynamic and transport simulation of the QGP dynamics [4, 127, 128].

The anisotropic ordering $\sigma_{\Delta\eta} > \sigma_{\Delta\phi}$ is preserved irrespective of Q_s , while the peak in $\sigma_{\Delta\eta}$ gets more pronounced with increasing Q_s . Both decorrelation increase with Q_s . Since the saturation momentum of the glasma directly dictates the strength of the color fields, one expects more decorrelation of the $Q\bar{Q}$ pairs with larger Q_s , as confirmed by our results.

C. Nuclear modification factor

1. Numerical R_{AA} (glasma simulations)

Using the procedures presented in Sec. III B, we simulate ensembles of heavy quark test particles initialized with a p_T distribution according to the FONLL calculation from Eq. (21) and follow their evolution in the glasma. As previously done in the literature [33–35], but now using SU(3) as a gauge group, we extract the nuclear modification factor in the glasma produced in an AA collision by initializing heavy quarks according to a pp input FONLL calculation, that is we numerically compute $dN/dp_T(\tau; pp)$ from Eq. (23). Additionally, we improve

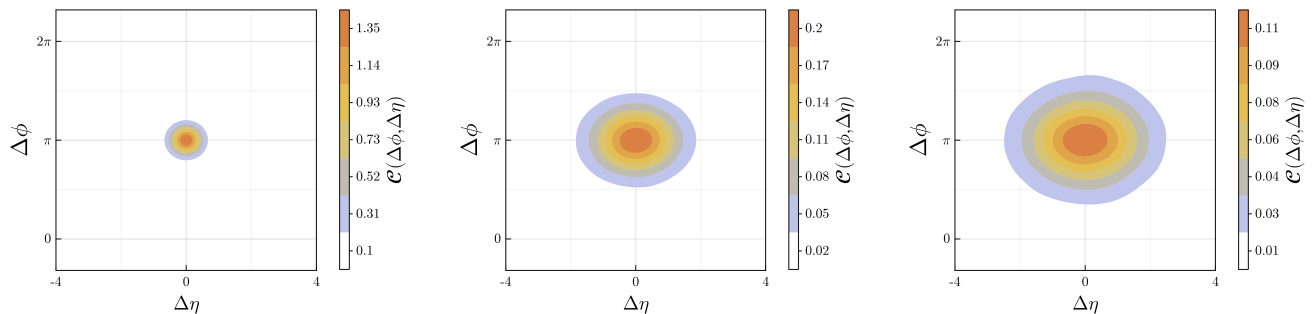


FIG. 5. The two-particle correlation $\mathcal{C}(\Delta\eta, \Delta\phi)$, as defined in Eq. (20), at different values of $\Delta\tau$, for a single glasma event of $Q_s = 2$ GeV with $N_{\text{tp}} = 10^5$ charm test particles initialized with fixed $p_T(\tau_{\text{form}}) = 1$ GeV. The *left panel* contains the almost initial highly peaked correlation, while the *middle panel* shows decorrelations in both $\Delta\eta$ and $\Delta\phi$. The *right panel* contains the correlation at $\Delta\tau = 0.3$ fm/c, the typical time at which the glasma stage at LHC ends. The magnitude of the correlation (color gradient) is extracted as a KDE and is not normalized.

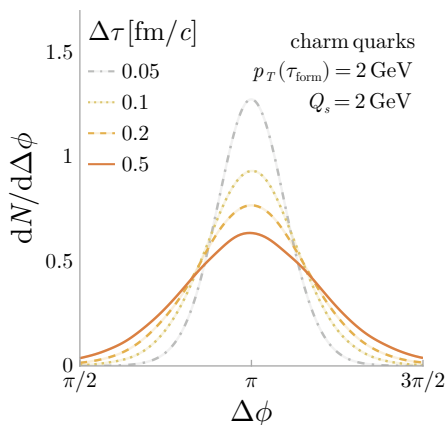


FIG. 6. Azimuthal angle decorrelation $\mathcal{C}(\Delta\phi)$, as expressed in Eq. (20), for charm quarks initialized with $p_T(\tau_{\text{form}}) = 2$ GeV. The decorrelation is extracted at various values of proper time $\Delta\tau \in \{0.05, 0.1, 0.2, 0.5\}$ fm/c (*different colors and line styles*).

this choice by using an initial FONLL spectrum in AA , which contains nuclear PDF effects, to initialize heavy quark production in the glasma, namely $dN/dp_T(\tau; AA)$ in Eq. (23). Unless otherwise specified, we extract R_{AA} using the former initialization with FONLL in pp in order to focus on the effect of the glasma phase. The default choice for the saturation momentum in glasma is $Q_s = 2$ GeV, the input FONLL calculation in pp corresponds to $\sqrt{s_{\text{pp}}} = 5.5$ TeV and the PDF choice CTEQ6.6.

The temporal evolution of $R_{AA}(p_T)$ is shown in Fig. 9 for both charm and beauty quarks, at various proper time regimes, namely the very-early stage $\tau = 0.1$ fm/c, the typical switching time to the subsequent stage $\tau = 0.3$ fm/c and the late stage $\tau = 1$ fm/c. The profile of R_{AA} is dictated by p_T migration from low to high p_T values, as revealed by the Gaussian broadening from the

toy model initialization with fixed p_T , see Fig. 3. This causes a depletion of particles in the small- p_T range of about $p_T < 2.5$ GeV for charm and $p_T < 4$ GeV for beauty quarks. Since the total number of quarks is conserved, the p_T migration causes an enhancement of R_{AA} at larger p_T . For beauty quarks, at sufficiently large p_T values, R_{AA} reaches a plateau as an effect of p_T migration equalization from larger and smaller p_T values, but for charm quarks R_{AA} starts to decrease at large p_T for later times τ .

At later times τ , the small- p_T migration followed by a large- p_T enhancement becomes more pronounced since the test particles get increasingly more deflected by the color force of the glasma fields. As previously observed in [50], since beauty quarks are formed earlier and thus experience stronger glasma fields, their p_T momentum broadening is larger than for charm quarks. Nevertheless, the outcome of our simulations is that R_{AA} is closer to identity for beauty quarks. This effect may be traced back to the p_T spectrum of charm quarks being steeper at large p_T , resulting in more p_T migration and consequently an enhanced R_{AA} as compared to beauty quarks.

The $\sqrt{s_{\text{pp}}}$ dependence of R_{AA} results from a combination of two separate effects. The collision energy $\sqrt{s_{\text{pp}}}$ influences the initial heavy quark spectrum in the FONLL calculation. On the other hand, also the saturation scale Q_s depends on $\sqrt{s_{\text{pp}}}$. We will first quantify these two effects separately, studying the dependence of R_{AA} on the initial $\sqrt{s_{\text{pp}}} \in \{2.75, 5.5, 7, 13\}$ TeV for fixed $Q_s = 2$ GeV and on $Q_s \in \{1, 1.5, 2, 2.5\}$ GeV using a given $\sqrt{s_{\text{pp}}} = 5.5$ TeV in the FONLL calculation, all with the same PDF set. The results depicted in Fig. 10 show a stronger dependence of R_{AA} on Q_s than on $\sqrt{s_{\text{pp}}}$. The FONLL spectra become less steep in the large- p_T tail with increasing collision energy $\sqrt{s_{\text{pp}}}$, yielding a smaller effect on the magnitude of R_{AA} . Increasing the saturation momentum Q_s produces stronger color fields, and thus generates larger p_T broadening and more enhance-

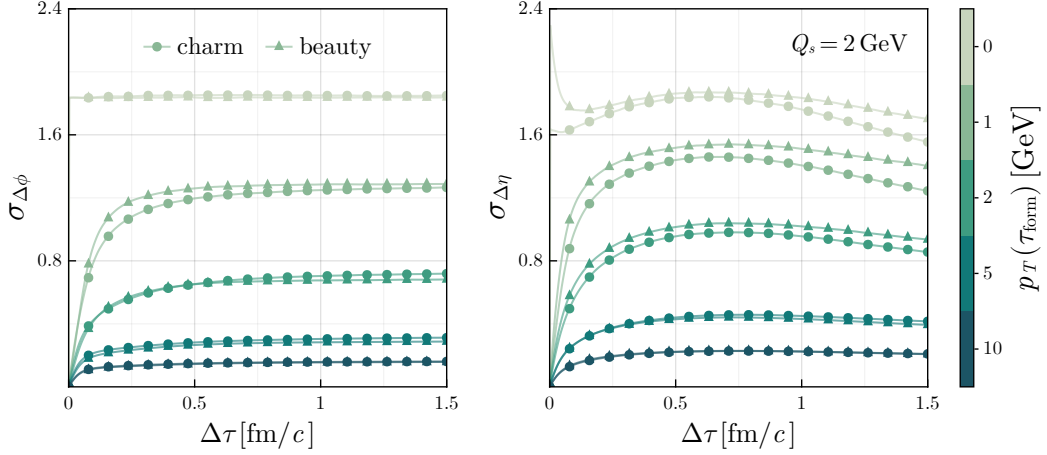


FIG. 7. Azimuthal $\sigma_{\Delta\phi}$ and rapidity $\sigma_{\Delta\eta}$ decorrelation widths, as a function of proper time $\Delta\tau$, for charm (*circle markers*) and beauty (*triangle markers*), initialized with $p_T(\tau_{\text{form}}) \in \{0, 1, 2, 5, 10\}$ GeV (*different colors*). In all these simulations, the glasma background field has $Q_s = 2$ GeV.

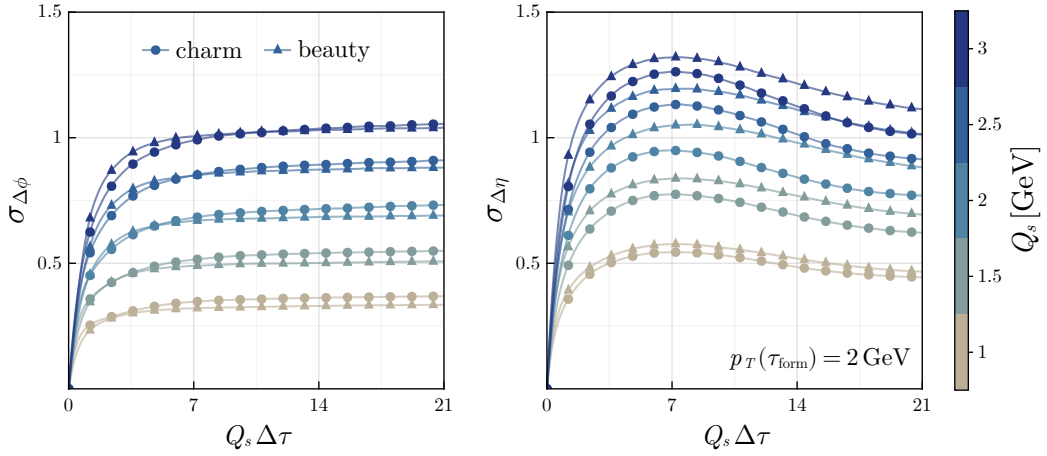


FIG. 8. Dependence of the decorrelation width in relative azimuthal angle $\sigma_{\Delta\phi}$ and rapidity $\sigma_{\Delta\eta}$ on the scaled dimensionless proper time $Q_s \Delta\tau$, for charm (*circle markers*) and beauty (*triangle markers*) quarks. The heavy quarks are initialized with the same $p_T = 2$ GeV but the glasma saturation momentum is varied $Q_s \in \{1, 1.5, 2, 2.5, 3\}$ GeV (*different colors*).

ment in R_{AA} .

To combine the two sources of \sqrt{s} -dependence of R_{AA} , we need to explicitly specify the dependence of the gluon saturation momentum Q_s on the collision energy \sqrt{s} . For this purpose, we use a mapping $\sqrt{s} \mapsto Q_s$ proposed in [91]. The nuclear saturation momentum scales according to a nuclear geometry factor with respect to the proton one $Q_{s,A}^2 \propto g(A)Q_{s,p}^2$, in which we choose $g(A) \propto A^{1/3}$ and neglect $\log A$ contributions. Within the GBW parametrization of the deep inelastic scattering (DIS) cross section [129], the proton saturation momentum may be parametrized in terms of the x momentum fraction of the parton as $Q_{s,p}^2 = Q_0^2(x_0/x)^\lambda$. The values of

the involved parameters are obtained from a fit to HERA data as $\lambda = 0.277$, $x_0 = 0.41 \cdot 10^{-4}$ and $Q_0 = 1$ GeV [129]. In practice, one chooses an effective x value for gluons as $x = x_{\text{eff}}$ where $x_{\text{eff}} \sim Q_s/\sqrt{s}$. Collecting all these parameterizations yields a mapping for the nuclear saturation momentum in terms of the collision energy which is valid up to a proportionality factor that may not be determined from our current setup. In this work, we choose to parametrize the saturation momentum as

$$Q_{s,A}^2 = A^{1/3}(Q_0^2 x_0^\lambda \sqrt{s}^\lambda)^{2/(2+\lambda)}. \quad (30)$$

We use this mapping and obtain the results shown in Fig. 11. Here one sees that the \sqrt{s} -dependences of the

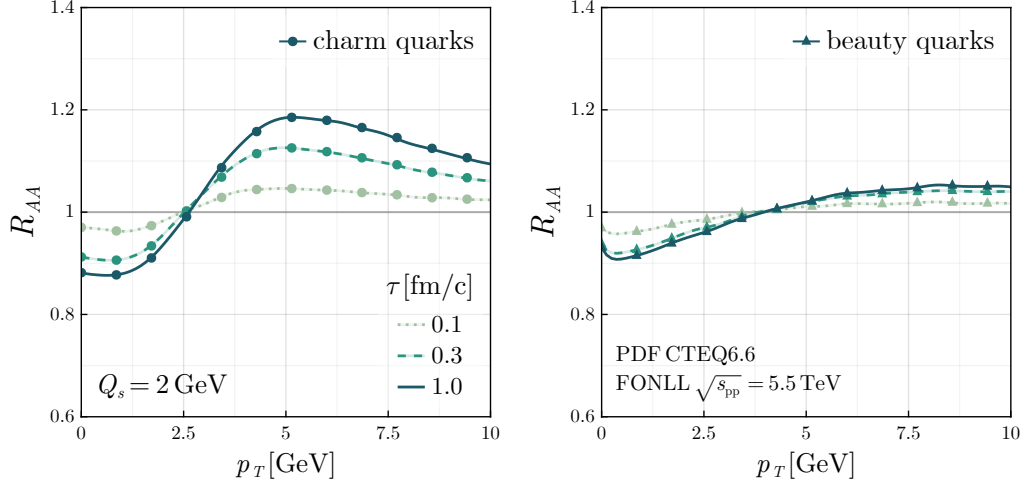


FIG. 9. Nuclear modification factor R_{AA} computed using Eq. (23), as a function of p_T , at various τ values (different colors and line styles). The results are shown for both charm (circle markers) and beauty (triangle markers) evolving in a glasma with $Q_s = 2$ GeV and produced according to the FONLL distribution from Eq. (21) using the PDF set CTEQ6.6 at the collision energy $\sqrt{s_{pp}} = 5.5$ TeV.

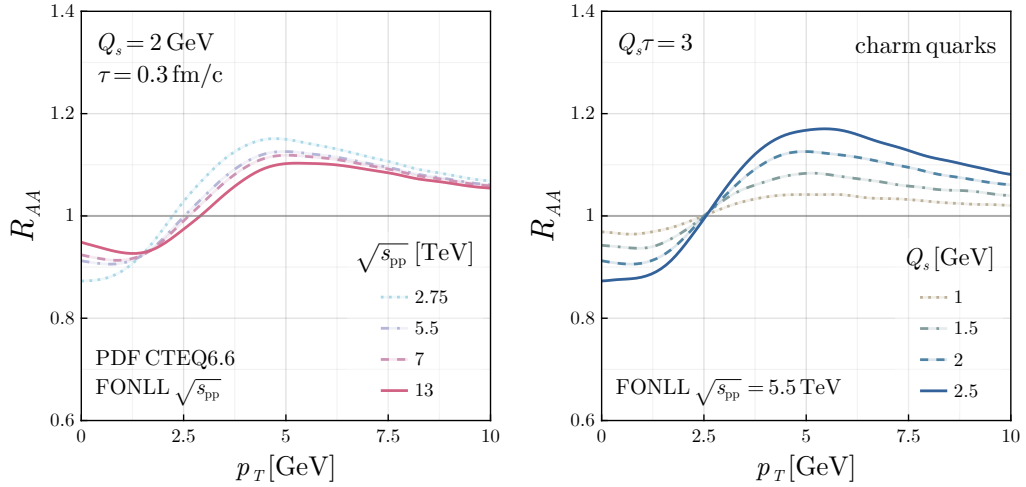


FIG. 10. Initial FONLL energy $\sqrt{s_{pp}}$ (left panel) and glasma saturation momentum Q_s (right panel) dependence of the nuclear modification factor $R_{AA}(p_T)$ for charm quarks. In the (left panel) R_{AA} is extracted at $\tau = 0.3$ fm/c with fixed glasma $Q_s = 2$ GeV and varying FONLL energy $\sqrt{s_{pp}}$ (different colors and line styles) for the PDF set CTEQ6.6, while in the (right panel) Q_s is varied (different colors and line styles) and R_{AA} is represented at fixed $Q_s\tau$ and FONLL energy $\sqrt{s_{pp}} = 5.5$ TeV and the same PDF set.

FONLL spectrum and Q_s partially cancel, resulting in a weak overall \sqrt{s} -dependence. In particular, the combined effect leads to very little variation of the magnitude of R_{AA} with \sqrt{s} , but to shift towards higher p_T . Comparing with the independent variations of Q_s and \sqrt{s} in the FONLL spectrum, one may infer that the \sqrt{s} -dependence in FONLL is a slightly stronger effect.

We can also account for nuclear PDF effects by initializing the heavy quark production probability density in the glasma $dN/dp_T(\tau; AA)$ with the FONLL calculation from Eqs. (21) and (22) for AA collisions. The results for

R_{AA} extracted using Eq. (23) for the combined nPDF + glasma effect are depicted in Fig. 12 and compared with the previous glasma extraction of R_{AA} using the glasma spectrum initialized with FONLL in pp , $dN/dp_T(\tau; pp)$, and with R_{AA} resulting solely from nuclear PDFs. The key finding is that the glasma p_T broadening enhances the nuclear effect. In both calculations including nPDFs, $R_{AA} < 1$ due to the nuclear shadowing phenomenon relevant in the small- x regime [123, 130, 131]. Since the overall effect of the glasma fields is to induce p_T -migration from low to high values, the p_T -differential slope of R_{AA}

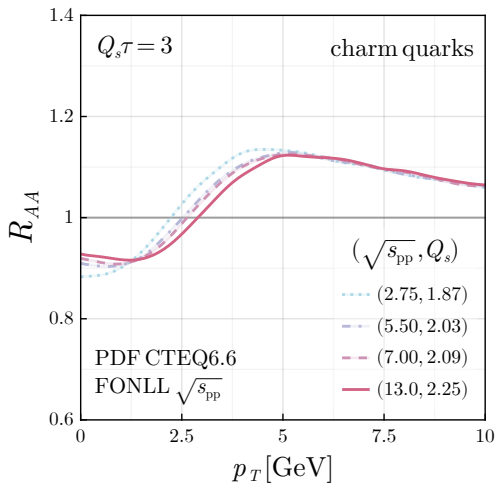


FIG. 11. Initial FONLL energy $\sqrt{s_{pp}}$ and saturation momentum Q_s dependence (*different colors and line styles*) of $R_{AA}(p_T)$, using the mapping from Eq. (30) for charm quarks at $Q_s\tau = 3$, using the PDF set CTEQ6.6.

is larger for the nPDF + glasma result compared to just the nPDF calculation. It was noted in [35] that glasma dynamics (already in SU(2)) would induce a shape of $R_{AA}(p_T)$ that increases with p_T which is opposite to what one would get considering heavy quark scatterings in the QGP already from $\tau = 0^+$. Here we have found that nPDF+glasma in SU(3) generate globally quite a stronger modification of $R_{AA}(p_T)$ than the one considered in [35]. This can be expected to significantly affect the quantitative estimates of the heavy quark space diffusion coefficient $D_s(T)$ and its relation to observables like $R_{AA}(p_T)$ and $v_2(p_T)$.

2. Analytical R_{AA} (toy model)

The Gaussian \vec{p}_T broadening toy model described in Sec. III B 2 allows the analytical extraction of R_{AA} defined in Eq. (25) using the glasma probability density proposed in Eq. (27). The only input required for this calculation is the width of the Gaussian broadening. For this purpose, we approximate σ with the standard deviation of the momentum kicks δp_T^2 expressed in Eq. (A1). We denote this width as σ_{p_T} and we extract it from numerical glasma simulations. For simplicity, we perform this extraction using charm quarks initialized with $p_T(\tau_{\text{form}}) = 0$ GeV which gives $\sigma_{p_T} = 0.64$ GeV and $p_T(\tau_{\text{form}}) = 10$ GeV for which $\sigma_{p_T} = 0.57$ GeV. The results for the analytical toy model R_{AA} are shown in Fig. 13 and compared with the numerical glasma R_{AA} . The shape of the p_T dependence is well reproduced while the magnitude slightly varies depending on the value of the Gaussian width σ_{p_T} . This result shows that, for reproducing R_{AA} , the Gaussian p_T broadening toy model

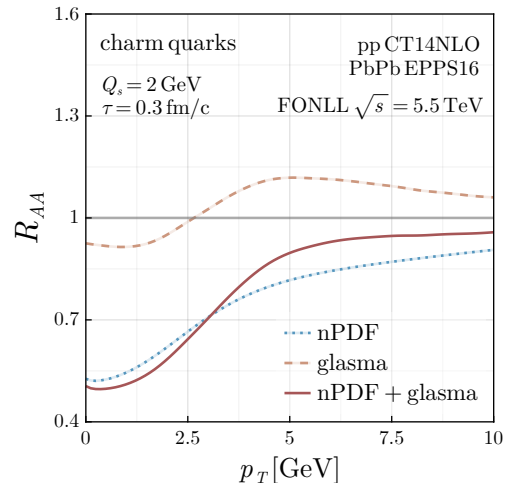


FIG. 12. Nuclear modification factor $R_{AA}(p_T)$ extracted from Eq. (23) using either the pp FONLL calculation with CT14NLO PDF as glasma input, labeled as *glasma*, or the AA FONLL calculation with EPPS16 nPDF in the glasma particle initialization, denoted as *nPDF+glasma*. The effect arising solely from nuclear effects in the FONLL calculation is also represented, with the label *nPDF*. The calculations are done for charm quarks evolving in a glasma with $Q_s = 2$ GeV, in a collision of $\sqrt{s} = 5.5$ TeV, at the proper time $\tau = 0.3$ fm/c.

captures the dynamics in the glasma phase.

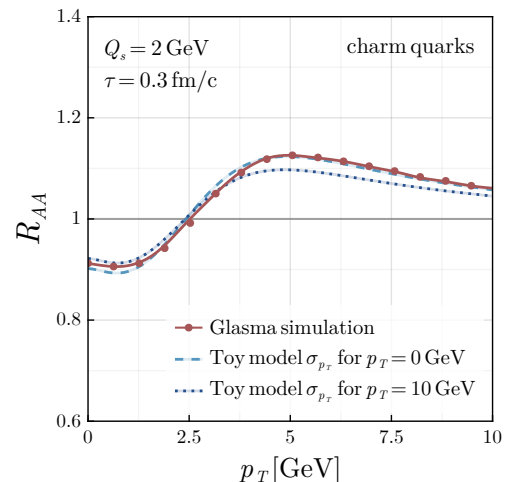


FIG. 13. Nuclear modification factor $R_{AA}(p_T)$ extracted from glasma simulations (*circle markers*) or from the analytical toy model using a Gaussian momentum exchange with fixed widths σ_{p_T} (*different styles of lines*). Results are shown for charm quarks at $\tau = 0.3$ fm/c in a glasma with $Q_s = 2$ GeV and a FONLL calculation with $\sqrt{s_{pp}} = 5.5$ TeV with the CTEQ6.6 PDF set.

V. CONCLUSION

We studied the phenomenological impact of the early-stage glasma fields on heavy quark angular correlations and transverse momentum spectra. Using our numerical solver for the transport of classical test particles in the non-Abelian Yang-Mills fields of the glasma, developed and tested in our previous work [50], we simulate ensembles of heavy quarks evolving in the glasma background fields. This study contains the first extraction of heavy quark two-particle correlations in the pre-equilibrium stage and a refined calculation of heavy quark R_{AA} including both glasma and nPDF effects.

Firstly, we extract the two-particle correlations of heavy quark Q and antiquark \bar{Q} pairs initially produced back-to-back in the glasma. We quantify how the glasma changes the initial correlation by extracting the rapidity $\sigma_{\Delta\eta}$ and azimuthal $\sigma_{\Delta\phi}$ correlation widths at different proper times $\Delta\tau$. Further, we systematically study the dependence of the decorrelation widths on the initial heavy quark p_T and glasma saturation momentum Q_s . Our results show that the glasma stage has a large effect on the two-particle correlations of low to moderate- p_T heavy quarks, causing a rapid decorrelation in both rapidity $\Delta\eta$ and relative azimuthal angle $\Delta\phi$. This effect gets more pronounced with increasing saturation momentum Q_s , since it encodes the strength of the glasma fields and thus the magnitude of the momentum kicks experienced by the heavy quarks. Our main finding is that the azimuthal correlation of $c\bar{c}$ pairs is significantly modified by the glasma phase. Since this result is only applicable in the early stage, combining our results with a modeling of the subsequent stages will be highly relevant for comparisons with experimental measurements. For example, the azimuthal correlations of $D\bar{D}$ pairs will be measured in heavy ion collisions at ALICE3 [132] to directly probe momentum broadening in the QGP, and azimuthal correlations of muons originating from heavy-flavor decays in PbPb collisions were reported by ATLAS [133].

Secondly, we investigated the effect of the glasma stage on the heavy quark nuclear modification factor R_{AA} . Earlier studies [33–35] evaluate either R_{AA} or R_{pA} in the glasma by initializing heavy quarks according to a p_T distribution given by the pQCD FONLL calculation in pp and then extract the resulting dN/dp_T in an SU(2) glasma. We improve these calculations by using SU(3) as a gauge group, initializing the heavy quark spectra with the FONLL calculation in both pp and AA . Our results qualitatively confirm the findings of these earlier works, namely that the glasma phase induces an overall p_T migration from small to large p_T for heavy quarks, causing $R_{AA} < 1$ at smaller- p_T and $R_{AA} > 1$ at larger- p_T , to conserve the total number of heavy quarks. Further, we study the dependence of R_{AA} on the saturation momentum Q_s and the initial collision energy \sqrt{s} in the FONLL calculation, along with a more realistic mapping between Q_s and \sqrt{s} inspired by DIS, and observe a large cancellation between the \sqrt{s} -dependences of the FONLL

spectrum and the value of Q_s . Additionally, we compare the numerically extracted R_{AA} with a toy model which assumes symmetric Gaussian \bar{p}_T broadenings. We find that such an approximation is only qualitatively in agreement with the results of the numerical simulations and can not replace the full glasma simulation. Lastly, we improve our framework by incorporating nPDF effects in the glasma R_{AA} . We achieve this by initializing heavy quark p_T spectra according to the FONLL cross-section in AA collisions, a calculation which includes nuclear PDF effects. Our results yield a combined nPDF+glasma $R_{AA} < 1$ caused by nuclear shadowing, and the nuclear modification is found to be more pronounced compared to the nPDF-only setup. This calculation for the heavy quark R_{AA} contains the most important initial stage effects, arising from CGC-inspired early-stage dynamics and nPDF considerations.

Our extraction of the two-particle correlations relies on simple glasma field configurations and toy model heavy quark test particle initialization. We plan to extend our analysis by including more sophisticated field and particle initial conditions. For the glasma fields produced in AA collisions, more realistic geometries may be achieved by incorporating finite-size effects. For this purpose, one may use an impact parameter b dependent MV model [134–137], where the initial MV color charge is sampled according to a Woods-Saxon impact parameter b -dependent distribution. This yields glasma fields whose energy density is contained within a finite simulation region. Additionally, we are interested in extending the $Q\bar{Q}$ angular decorrelation study to small systems, for which there is experimental data on $D\bar{D}$ angular correlations in either pp [138–142] or pA [142, 143]. For this purpose, we plan to incorporate proton geometry [135, 144–146] in our glasma implementation. With this setup, one could further study the effect on the two-particle correlations of nucleonic and sub-nucleonic fluctuations or hot spots in the high-energy proton [137, 145, 147, 148].

The toy model initialization for the heavy quark coordinate and momenta may also be improved. A more realistic coordinate distribution can also be implemented by producing the quarks according to the initial energy density profile of the glasma fields. This will become more important when considering smaller systems like pp or pA collisions and finer geometry details like fluctuations or hot spots. Additionally, one could use a heavy-ion event generator such as Pythia Angantyr [149] to input the p_T and angular $\Delta\phi$ distributions of heavy quark $Q\bar{Q}$ pairs in the evolving glasma fields produced in AA collisions. Lastly, one additional effect arising from finite-size effects in the glasma is that the $Q\bar{Q}$ pairs may experience a different decorrelation since at least one of the quarks from the pair could in principle “escape” the highly dense medium. This will require a more sophisticated modeling of the glasma transverse density profile which will produce a different angular decorrelation for $Q\bar{Q}$ pairs evolving in this profile. Such an implementation would be of interest for further studies.

One may go beyond the boost-invariant approximation implemented at the level of the glasma fields employed in the current study, by evolving the glasma fields in a full 3+1D setup [150–159]. Such an improvement will enable the study of the 3D angular decorrelation of the $Q\bar{Q}$ pairs in a 3+1D background field and will provide more reliable results for the rapidity dependence of $\mathcal{C}(\Delta\eta)$. Moreover, beyond the extraction of the two-particle correlation, the effect of the rapidity-dependent glasma fields on the transport of both heavy quarks and jets in the glasma represents a promising direction for future research.

Another shortcoming of the current study is the lack of an energy loss mechanisms for the heavy quarks. The glasma fields induce a significant momentum broadening for both heavy quarks and jets. Such a momentum broadening causes gluon emission leading to radiative energy loss, which is not accounted for in our present formalism. However, it would be highly desirable to incorporate more realistic energy loss mechanisms in our current framework. For this purpose, the calculations developed for classical gluon radiation from a point particle propagating in CGC fields [160–162] may provide additional insight. Alternatively, one may take inspiration from the energy loss formalism recently developed in [68] for jets in a glasma background field, based on synchrotron gluon radiation [163, 164]. Lastly, energy loss via gluon emissions may be included by using the framework developed for the quantum evolution of a jet in a classical background field [165–167]. Such methods will enable us to study the effect of the glasma fields on the energy loss of hard probes and to quantify it by extracting, for example, the nuclear modification factor R_{AA} . Additionally, energy loss effects will be crucial for understanding the jet evolution and in-medium radiation in the early-stages.

Lastly, it would be of great interest to couple these early-time predictions with the subsequent stages of heavy-ion collisions. Earlier model estimates performed using kinetic theory [52–54], which is applicable after the glasma stage, managed to couple the transport coefficients κ for heavy quarks and \hat{q} for jets. Nevertheless, the very-early stage contribution to the azimuthal correlation $\mathcal{C}(\Delta\phi)$ and nuclear modification factor R_{AA} has not been yet accounted for in a systematic manner in both the glasma and QGP phases. In order to compare to finally measured experimental data, model calculations would require simultaneously coupling multiple stages for both the medium and the hard probes: the glasma background fields to kinetic theory or hydrodynamics, the transport of the hard probes in glasma to other transport models applicable during the QGP phase, and the interaction of the hard probes with the underlying medium throughout its evolution. Even though a complete unification of all stages is not yet feasible, our current approach may be extended to provide an improved input to kinetic theory. Coupling the glasma to kinetic theory may be achieved by extracting the gluon distribution function of the glasma fields, as previously done in [168, 169]. For the hard probes, including a colli-

sion term in the Boltzmann-Vlasov equation used for the classical transport of the probes would provide a more correct treatment of the interactions between the hard degrees of freedom [109–111, 170, 171].

ACKNOWLEDGMENTS

We are grateful to I. Helenius and H. Paukkunen for very helpful discussions about heavy quark production, the FONLL calculation, and nPDFs. D.A. is grateful to Pol-Bernard Gossiaux for insightful discussions about $D\bar{D}$ correlations. This work was supported by the Research Council of Finland, the Centre of Excellence in Quark Matter (projects 346324 and 364191), and projects 338263, 346567, and 359902 (H.M). D.A. acknowledges the support of the Vilho, Yrjö and Kalle Väisälä Foundation. D.M. acknowledges support from the Austrian Science Fund (FWF) projects P 34764 and P 34455. This work was also supported under the European Union’s Horizon 2020 research and innovation programme by the European Research Council (ERC, grant agreements No. ERC-2023-101123801 GlueSatLight and ERC-2018-ADG-835105 YoctoLHC) and by the STRONG-2020 project (grant agreement No. 824093). The content of this article does not reflect the official opinion of the European Union and responsibility for the information and views expressed therein lies entirely with the authors. Computing resources from CSC – IT Center for Science in Espoo, Finland and the Finnish Grid and Cloud Infrastructure (persistent identifier urn:nbn:fi:research-infras-2016072533) were used in this work.

Appendix A: Classical Casimir invariants

1. Casimir scaling

As expressed in Eq. (12), the heavy quark color charge $Q(\tau)$ is obtained by applying color rotations to an initial color charge vector $Q(\tau_0) \equiv Q_0$. The color components of the initial color charge $Q_0 = Q_0^a T^a$ obey the Casimir invariant constraints from Eq. (14), namely $q_2(R) = Q_0^a Q_0^a$ and $q_3(R) = d_{abc} Q_0^a Q_0^b Q_0^c$. The values of the quadratic q_2 and cubic q_3 Casimir invariants are unique to the representation R . As discussed in Sec. IV A, for quarks which lie in the $R = F$ fundamental representation, we choose $q_2 = C_2(F)$, with $C_2(F) = (N_c^2 - 1)/(2N_c)$ the group theory quadratic Casimir in the fundamental representation of $SU(N_c)$, and $q_3 = 0$.

There exists an arbitrariness in choosing the values for the classical Casimirs. A natural choice would be to fix their values to the group theory Casimirs. Nevertheless, as noticed in our previous work [50], there is no way to construct real classical color charge components Q_0^a whose classical Casimirs correspond to the standard group theory values, namely both $q_{2,3}(R) \neq C_{2,3}(R)$.

Nevertheless, it has been observed [50, 104–106, 172] that for the choice $q_{2,3}(R) = D_R C_{2,3}(R)$, where D_R is the dimension of the representation, one can sample such classical color charges.

This choice consequently affects any classical quantities extracted using the classical color charges. Most importantly, using arbitrary classical Casimirs invariants yields classical quantities which do not map to their quantum analogues, extracted using group theory Casimirs. In [50], we analyzed such a quantity, more precisely the momentum broadening defined as

$$\delta p_i^2(\tau) \equiv p_i^2(\tau) - p_i^2(\tau_{\text{form}}) \quad (\text{A1})$$

for each component $i = x, y, z$ and then averaged $\langle \delta p_i^2 \rangle$ over multiple glasma and particle configurations. We noticed its special scaling property

$$\langle \delta p_i^2 \rangle_R \propto q_2(R) \quad (\text{A2})$$

in terms of the classical quadratic Casimir $q_2(R)$. Starting from the initial choice $q_{2,3} = D_R C_{2,3}(R)$, we used this scaling and obtained an expression for extracting the momentum broadening corresponding to group theory Casimirs as $\langle p_i^2 \rangle_R / D_R$. Nevertheless, this mapping was derived only for momentum broadening of either infinitely massive or highly energetic quarks and is thus not applicable to other quantities, such as p_T -spectra or correlation widths, and heavy quarks beyond the infinite mass approximation.

2. Effect of cubic Casimir

The Casimir scaling of the momentum broadening from Eq. (A2), observed in limiting cases, suggests that the cubic Casimir q_3 does not affect, or only very weakly affects, the particle momenta. Inspired by this scaling, we investigate whether the classical quantities of interest for us in this study, such as the components of the momentum broadening for quarks in any kinematic regime, the widths of two-particle correlations and the nuclear modification factor, exhibit any dependence on the cubic Casimir q_3 . A lack of dependence on q_3 implies that the effect of the classical color algebra is primarily given by q_2 . Thus, one may fix $q_2 = C_2(F)$ and $q_3 = 0$, which will yield values compatible with the quantum calculations. To this end, we study how the aforementioned classical quantities depend on the variation of q_3 . Further, we show only the dependence of the momentum broadening and decorrelation widths on the choice of q_3 , by keeping

q_2 fixed with either $q_2 = D_F C_2(F) = 4$ as done in [50], or $q_2 = C_2(F) = 4/3$ for SU(3).

a. Momentum broadening

The dependence on q_3 of the longitudinal L and transverse T components of the momentum broadening for charm quarks initialized with $p_T(\tau_{\text{form}}) = 2$ GeV is shown in Fig. 14, using either $q_2 = 4$ or $q_2 = 4/3$. First, we generate a large ensemble of classical color charge configurations $\{Q^a\}_a$ for $a \in \overline{1,8}$ with fixed q_2 and no constraint on q_3 . This is done by distributing the color components Q^a on an 8-dimensional hypersphere of radius given by q_2 and then extracting q_3 according to Eq. (14). The resulting KDE built using all numerical values of q_3 is shown in the inset plots from Fig. 14 and reveals that most classical color charges have a null cubic Casimir $q_3 = 0$. Using a discrete subset of q_3 values, we study the effect of varying q_3 by keeping q_2 fixed, for both $q_2 = 4$ and $q_2 = 4/3$. In both cases, the momentum broadening components show a very weak dependence on q_3 , with the longitudinal component being more affected at later $\Delta\tau$ times. Lastly, we indirectly test the validity of the Casimir scaling property from Eq. (A2). In case of Casimir scaling, the ratio $\langle \delta p^2 \rangle / D_F$ for $q_2 = D_F C_2(F)$ should directly match $\langle \delta p^2 \rangle$ obtained with $q_2 = C_2$. Nevertheless, our numerical results reveal a weak deviation from Casimir scaling for $\langle \delta p_L^2 \rangle$. Interestingly, we separately checked that, as the heavy quark dynamics is further away from the infinite mass static quark scenario, this deviation becomes more pronounced. Violations of Casimir scaling have also been reported for jet quarks propagating in-medium as opposed to in-vacuum [173].

b. Decorrelation width

As similarly done for the momentum broadening, we study the q_3 dependence of the azimuthal $\sigma_{\Delta\phi}$ and rapidity $\sigma_{\Delta\eta}$ correlation widths, for charm quarks initialized with $p_T(\tau_{\text{form}}) = 2$ GeV. The results from Fig. 15 show the $\Delta\tau$ evolution of these widths for $q_2 = 4$ and $q_2 = 4/3$, by varying q_3 with the same set of discrete values used for the momentum broadening. As for $\langle \delta p^2 \rangle$, the widths $\sigma_{\Delta\eta, \Delta\phi}$ exhibit a weak dependence on q_3 , with the exception of $\sigma_{\Delta\eta}$ for $q_2 = 4$ at larger $\Delta\tau$ values. Nevertheless, such deviations are not problematic since at such late times, the glasma picture becomes unreliable.

[1] W. Busza, K. Rajagopal and W. van der Schee, *Heavy Ion Collisions: The Big Picture, and the Big Questions*, *Ann. Rev. Nucl. Part. Sci.* **68** (2018) 339 [[arXiv:1802.04801](https://arxiv.org/abs/1802.04801)] [[hep-ph](#)].

[2] E. V. Shuryak, *What RHIC experiments and theory tell us about properties of quark-gluon plasma?*, *Nucl. Phys. A* **750** (2005) 64 [[arXiv:hep-ph/0405066](https://arxiv.org/abs/hep-ph/0405066)].

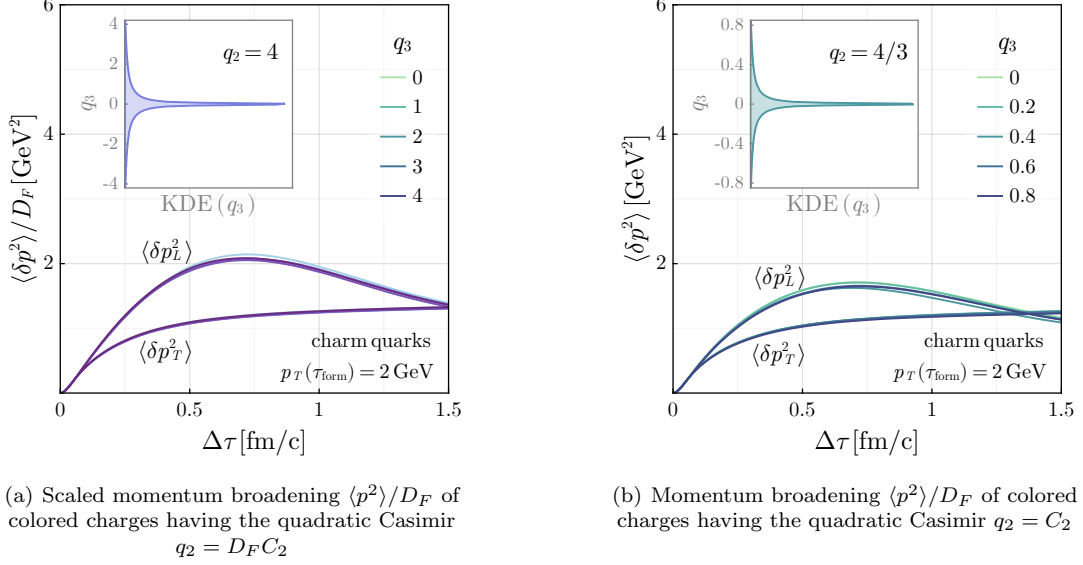


FIG. 14. Proper time $\Delta\tau$ evolution of the longitudinal $\langle \delta p_L^2 \rangle$ and transverse $\langle \delta p_T^2 \rangle$ components of the momentum broadening for charm quarks with $p_T(\tau_{\text{form}}) = 2 \text{ GeV}$. The corresponding classical colored charges are initialized with fixed quadratic Casimir $q_2 = 4$ (left) and $q_2 = 4/3$ (right), while the cubic Casimir q_3 is allowed to vary. From all the possible values for q_3 , as represented in the KDE from the (insets), a few representative ones are chosen to be varied.

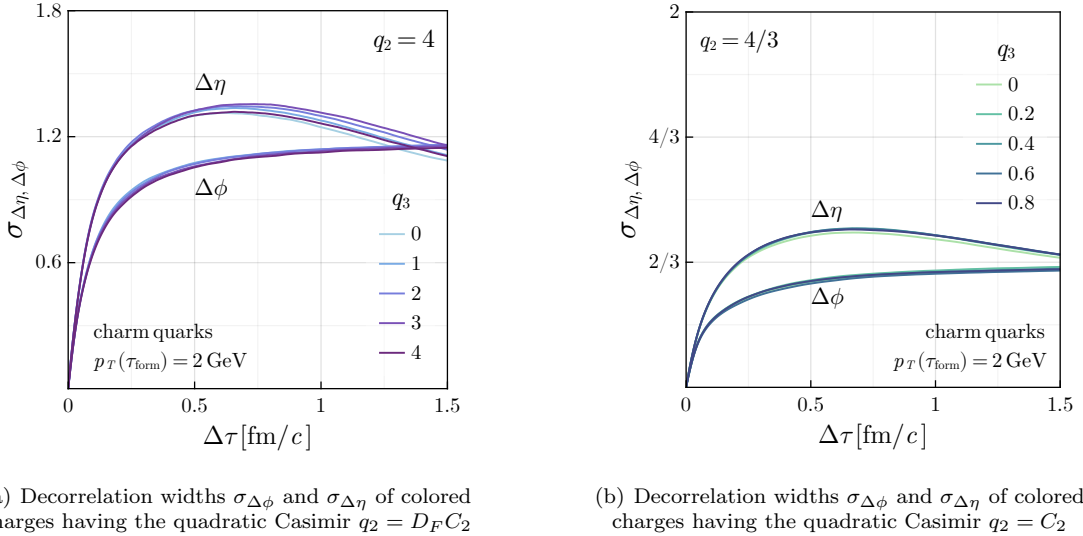


FIG. 15. Proper time $\Delta\tau$ evolution of the decorrelation width in relative azimuthal angle $\sigma_{\Delta\phi}$ and pseudorapidity $\sigma_{\Delta\eta}$ for charm anticharm pairs initialized with $p_T(\tau_{\text{form}}) = 2 \text{ GeV}$. As in Fig. 14, the cubic Casimir q_3 is varied while keeping the quadratic Casimir with the fixed values of $q_2 = 4$ (left) and $q_2 = 4/3$ (right).

- [3] J. P. Blaizot and A. H. Mueller, *The Early Stage of Ultrarelativistic Heavy Ion Collisions*, *Nucl. Phys. B* **289** (1987) 847.
- [4] U. Heinz and R. Snellings, *Collective flow and viscosity in relativistic heavy-ion collisions*, *Ann. Rev. Nucl. Part. Sci.* **63** (2013) 123 [[arXiv:1301.2826](#) [[nucl-th](#)]].
- [5] U. W. Heinz, *Towards the Little Bang Standard Model*, *J. Phys. Conf. Ser.* **455** (2013) 012044 [[arXiv:1304.3634](#) [[nucl-th](#)]].
- [6] C. Gale, S. Jeon and B. Schenke, *Hydrodynamic Modeling of Heavy-Ion Collisions*, *Int. J. Mod. Phys. A* **28** (2013) 1340011 [[arXiv:1301.5893](#) [[nucl-th](#)]].
- [7] A. Kurkela and Y. Zhu, *Isotropization and hydrodynamization in weakly coupled heavy-ion collisions*, *Phys. Rev. Lett.* **115** (2015) no. 18 182301 [[arXiv:1506.06647](#) [[hep-ph](#)]].

- [8] F. Gelis, *Some Aspects of the Theory of Heavy Ion Collisions*, *Rept. Prog. Phys.* **84** (2021) no. 5 056301 [[arXiv:2102.07604](#) [[hep-ph](#)]].
- [9] J. Auvinen, J. E. Bernhard, S. A. Bass and I. Karpenko, *Investigating the collision energy dependence of η/s in the beam energy scan at the BNL Relativistic Heavy Ion Collider using Bayesian statistics*, *Phys. Rev. C* **97** (2018) no. 4 044905 [[arXiv:1706.03666](#) [[hep-ph](#)]].
- [10] G. Nijs, W. van der Schee, U. Gürsoy and R. Snellings, *Bayesian analysis of heavy ion collisions with the heavy ion computational framework Trajectum*, *Phys. Rev. C* **103** (2021) no. 5 054909 [[arXiv:2010.15134](#) [[nucl-th](#)]].
- [11] **JETSCAPE** collaboration, D. Everett *et al.*, *Multisystem Bayesian constraints on the transport coefficients of QCD matter*, *Phys. Rev. C* **103** (2021) no. 5 054904 [[arXiv:2011.01430](#) [[hep-ph](#)]].
- [12] H. van Hees, V. Greco and R. Rapp, *Heavy-quark probes of the quark-gluon plasma at RHIC*, *Phys. Rev. C* **73** (2006) 034913 [[arXiv:nucl-th/0508055](#)].
- [13] P. B. Gossiaux and J. Aichelin, *Towards an understanding of the RHIC single electron data*, *Phys. Rev. C* **78** (2008) 014904 [[arXiv:0802.2525](#) [[hep-ph](#)]].
- [14] J. Uphoff, O. Fochler, Z. Xu and C. Greiner, *Open Heavy Flavor in Pb+Pb Collisions at $\sqrt{s} = 2.76$ TeV within a Transport Model*, *Phys. Lett. B* **717** (2012) 430 [[arXiv:1205.4945](#) [[hep-ph](#)]].
- [15] S. Cao, G.-Y. Qin and S. A. Bass, *Energy loss, hadronization and hadronic interactions of heavy flavors in relativistic heavy-ion collisions*, *Phys. Rev. C* **92** (2015) no. 2 024907 [[arXiv:1505.01413](#) [[nucl-th](#)]].
- [16] F. Scardina, S. K. Das, V. Minissale, S. Plumari and V. Greco, *Estimating the charm quark diffusion coefficient and thermalization time from D meson spectra at energies available at the BNL Relativistic Heavy Ion Collider and the CERN Large Hadron Collider*, *Phys. Rev. C* **96** (2017) no. 4 044905 [[arXiv:1707.05452](#) [[nucl-th](#)]].
- [17] F. Prino and R. Rapp, *Open Heavy Flavor in QCD Matter and in Nuclear Collisions*, *J. Phys. G* **43** (2016) no. 9 093002 [[arXiv:1603.00529](#) [[nucl-ex](#)]].
- [18] X. Dong and V. Greco, *Heavy quark production and properties of Quark-Gluon Plasma*, *Prog. Part. Nucl. Phys.* **104** (2019) 97.
- [19] D. d'Enterria, *Jet quenching*, *Landolt-Bornstein* **23** (2010) 471 [[arXiv:0902.2011](#) [[nucl-ex](#)]].
- [20] L. Apolinário, Y.-J. Lee and M. Winn, *Heavy quarks and jets as probes of the QGP*, *Prog. Part. Nucl. Phys.* **127** (2022) 103990 [[arXiv:2203.16352](#) [[hep-ph](#)]].
- [21] Y. Xu *et al.*, *Resolving discrepancies in the estimation of heavy quark transport coefficients in relativistic heavy-ion collisions*, *Phys. Rev. C* **99** (2019) no. 1 014902 [[arXiv:1809.10734](#) [[nucl-th](#)]].
- [22] S.-Q. Li, W.-J. Xing, F.-L. Liu, S. Cao and G.-Y. Qin, *Heavy flavor quenching and flow: the roles of initial condition, pre-equilibrium evolution, and in-medium interaction*, *Chin. Phys. C* **44** (2020) no. 11 114101 [[arXiv:2005.03330](#) [[nucl-th](#)]].
- [23] E. Iancu, A. Leonidov and L. D. McLerran, *Nonlinear gluon evolution in the color glass condensate. 1.*, *Nucl. Phys. A* **692** (2001) 583 [[arXiv:hep-ph/0011241](#)].
- [24] E. Iancu and R. Venugopalan in *Quark-gluon plasma 4* (R. C. Hwa and X.-N. Wang, eds.), pp. 249–363. World Scientific, 2003. [[arXiv:hep-ph/0303204](#)].
- [25] E. Iancu, *Physics of the Color Glass Condensate*. PhD thesis, IPhT, Saclay, 2005.
- [26] F. Gelis, E. Iancu, J. Jalilian-Marian and R. Venugopalan, *The Color Glass Condensate*, *Ann. Rev. Nucl. Part. Sci.* **60** (2010) 463 [[arXiv:1002.0333](#) [[hep-ph](#)]].
- [27] F. Gelis, *Color Glass Condensate and Glasma*, *Int. J. Mod. Phys. A* **28** (2013) 1330001 [[arXiv:1211.3327](#) [[hep-ph](#)]].
- [28] A. Kovner, L. D. McLerran and H. Weigert, *Gluon production from non-Abelian Weizsacker-Williams fields in nucleus-nucleus collisions*, *Phys. Rev. D* **52** (1995) 6231 [[arXiv:hep-ph/9502289](#)].
- [29] T. Lappi and L. McLerran, *Some features of the glasma*, *Nucl. Phys. A* **772** (2006) 200 [[arXiv:hep-ph/0602189](#)].
- [30] K. Fukushima and F. Gelis, *The evolving Glasma*, *Nucl. Phys. A* **874** (2012) 108 [[arXiv:1106.1396](#) [[hep-ph](#)]].
- [31] S. K. Das, M. Ruggieri, S. Mazumder, V. Greco and J.-e. Alam, *Heavy quark diffusion in the pre-equilibrium stage of heavy ion collisions*, *J. Phys. G* **42** (2015) no. 9 095108 [[arXiv:1501.07521](#) [[nucl-th](#)]].
- [32] S. K. Das, M. Ruggieri, F. Scardina, S. Plumari and V. Greco, *Effect of pre-equilibrium phase on R_{AA} and v_2 of heavy quarks in heavy ion collisions*, *J. Phys. G* **44** (2017) no. 9 095102 [[arXiv:1701.05123](#) [[nucl-th](#)]].
- [33] M. Ruggieri and S. K. Das, *Cathode tube effect: Heavy quarks probing the glasma in p-Pb collisions*, *Phys. Rev. D* **98** (2018) no. 9 094024 [[arXiv:1805.09617](#) [[nucl-th](#)]].
- [34] J. H. Liu, S. Plumari, S. K. Das, V. Greco and M. Ruggieri, *Diffusion of heavy quarks in the early stage of high-energy nuclear collisions at energies available at the BNL Relativistic Heavy Ion Collider and at the CERN Large Hadron Collider*, *Phys. Rev. C* **102** (2020) no. 4 044902 [[arXiv:1911.02480](#) [[nucl-th](#)]].
- [35] Y. Sun, G. Coci, S. K. Das, S. Plumari, M. Ruggieri and V. Greco, *Impact of Glasma on heavy quark observables in nucleus-nucleus collisions at LHC*, *Phys. Lett. B* **798** (2019) 134933 [[arXiv:1902.06254](#) [[nucl-th](#)]].
- [36] J.-H. Liu, S. K. Das, V. Greco and M. Ruggieri, *Ballistic diffusion of heavy quarks in the early stage of relativistic heavy ion collisions at RHIC and the LHC*, *Phys. Rev. D* **103** (2021) no. 3 034029 [[arXiv:2011.05818](#) [[hep-ph](#)]].
- [37] P. Khowal, S. K. Das, L. Oliva and M. Ruggieri, *Heavy quarks in the early stage of high energy nuclear collisions at RHIC and LHC: Brownian motion versus diffusion in the evolving Glasma*, *Eur. Phys. J. Plus* **137** (2022) no. 3 307 [[arXiv:2110.14610](#) [[hep-ph](#)]].
- [38] M. Ruggieri, Pooja, J. Prakash and S. K. Das, *Memory effects on energy loss and diffusion of heavy quarks in the quark-gluon plasma*, *Phys. Rev. D* **106** (2022) no. 3 034032 [[arXiv:2203.06712](#) [[hep-ph](#)]].
- [39] Pooja, S. K. Das, V. Greco and M. Ruggieri, *Anisotropic fluctuations of angular momentum of*

- heavy quarks in the Glasma, *Eur. Phys. J. Plus* **138** (2023) no. 4 313 [[arXiv:2212.09725 \[hep-ph\]](#)].
- [40] Pooja, M. Y. Jamal, P. P. Bhaduri, M. Ruggieri and S. K. Das, $c\bar{c}$ and $b\bar{b}$ suppression in Glasma, [arXiv:2404.05315 \[hep-ph\]](#).
- [41] S. Cao, G.-Y. Qin and S. A. Bass, Heavy-quark dynamics and hadronization in ultrarelativistic heavy-ion collisions: Collisional versus radiative energy loss, *Phys. Rev. C* **88** (2013) 044907 [[arXiv:1308.0617 \[nucl-th\]](#)].
- [42] S. Cao et. al., Toward the determination of heavy-quark transport coefficients in quark-gluon plasma, *Phys. Rev. C* **99** (2019) no. 5 054907 [[arXiv:1809.07894 \[nucl-th\]](#)].
- [43] A. Ipp, D. I. Müller and D. Schuh, Anisotropic momentum broadening in the 2+1D Glasma: analytic weak field approximation and lattice simulations, *Phys. Rev. D* **102** (2020) no. 7 074001 [[arXiv:2001.10001 \[hep-ph\]](#)].
- [44] A. Ipp, D. I. Müller and D. Schuh, Jet momentum broadening in the pre-equilibrium Glasma, *Phys. Lett. B* **810** (2020) 135810 [[arXiv:2009.14206 \[hep-ph\]](#)].
- [45] M. E. Carrington, A. Czajka and S. Mrowczynski, Heavy Quarks Embedded in Glasma, *Nucl. Phys. A* **1001** (2020) 121914 [[arXiv:2001.05074 \[nucl-th\]](#)].
- [46] M. E. Carrington, A. Czajka and S. Mrowczynski, Jet quenching in glasma, *Phys. Lett. B* **834** (2022) 137464 [[arXiv:2112.06812 \[hep-ph\]](#)].
- [47] M. E. Carrington, A. Czajka and S. Mrowczynski, Transport of hard probes through glasma, *Phys. Rev. C* **105** (2022) no. 6 064910 [[arXiv:2202.00357 \[nucl-th\]](#)].
- [48] M. E. Carrington, W. N. Cowie, B. T. Friesen, S. Mrowczynski and D. Pickering, Glasma properties in small proper-time expansion, *Phys. Rev. C* **108** (2023) no. 5 054903 [[arXiv:2304.03241 \[nucl-th\]](#)].
- [49] M. E. Carrington and S. Mrowczynski in *63rd Cracow School of Theoretical Physics: Nuclear Matter at Extreme Densities and High Temperatures*, 1, 2024. [arXiv:2401.13705 \[nucl-th\]](#).
- [50] D. Avramescu, V. Băran, V. Greco, A. Ipp, D. I. Müller and M. Ruggieri, Simulating jets and heavy quarks in the glasma using the colored particle-in-cell method, *Phys. Rev. D* **107** (2023) no. 11 114021 [[arXiv:2303.05599 \[hep-ph\]](#)].
- [51] D. Avramescu, V. Băran, V. Greco, A. Ipp, D. I. Müller and M. Ruggieri, Heavy quark κ and jet \hat{q} transport coefficients in the Glasma early stage of heavy-ion collisions, *PoS HardProbes2023* (2024) 056 [[arXiv:2307.07999 \[hep-ph\]](#)].
- [52] K. Boguslavski, A. Kurkela, T. Lappi, F. Lindenbauer and J. Peuron, Jet momentum broadening during initial stages in heavy-ion collisions, *Phys. Lett. B* **850** (2024) 138525 [[arXiv:2303.12595 \[hep-ph\]](#)].
- [53] K. Boguslavski, A. Kurkela, T. Lappi, F. Lindenbauer and J. Peuron, Heavy quark diffusion coefficient in heavy-ion collisions via kinetic theory, *Phys. Rev. D* **109** (2024) no. 1 014025 [[arXiv:2303.12520 \[hep-ph\]](#)].
- [54] K. Boguslavski, A. Kurkela, T. Lappi, F. Lindenbauer and J. Peuron, Jet quenching parameter in QCD kinetic theory, [arXiv:2312.00447 \[hep-ph\]](#).
- [55] X. Du, Heavy quark drag and diffusion coefficients in the prehydrodynamic QCD plasma, *Phys. Rev. C* **109** (2024) no. 1 014901 [[arXiv:2306.02530 \[hep-ph\]](#)].
- [56] F. Zhou, J. Brewer and A. Mazeliauskas, Minijet quenching in non-equilibrium quark-gluon plasma, *JHEP* **06** (2024) 214 [[arXiv:2402.09298 \[hep-ph\]](#)].
- [57] K. Boguslavski, A. Kurkela, T. Lappi and J. Peuron, Spectral function for overoccupied gluodynamics from real-time lattice simulations, *Phys. Rev. D* **98** (2018) no. 1 014006 [[arXiv:1804.01966 \[hep-ph\]](#)].
- [58] K. Boguslavski, A. Kurkela, T. Lappi and J. Peuron, Heavy quark diffusion in an overoccupied gluon plasma, *JHEP* **09** (2020) 077 [[arXiv:2005.02418 \[hep-ph\]](#)].
- [59] K. Boguslavski, A. Kurkela, T. Lappi and J. Peuron, Heavy quark momentum diffusion coefficient in 3D gluon plasma, *Nucl. Phys. A* **1005** (2021) 121970 [[arXiv:2001.11863 \[hep-ph\]](#)].
- [60] L. Backfried, K. Boguslavski and P. Hotzy, Heavy-quark diffusion in 2+1D and Glasma-like plasmas: evidence of a transport peak, [arXiv:2408.12646 \[hep-ph\]](#).
- [61] H. Pandey, S. Schlichting and S. Sharma, Heavy-Quark Momentum Broadening in a Non-Abelian Plasma away from Thermal Equilibrium, *Phys. Rev. Lett.* **132** (2024) no. 22 222301 [[arXiv:2312.12280 \[hep-lat\]](#)].
- [62] S. Hauksson, S. Jeon and C. Gale, Momentum broadening of energetic partons in an anisotropic plasma, *Phys. Rev. C* **105** (2022) no. 1 014914 [[arXiv:2109.04575 \[hep-ph\]](#)].
- [63] S. Hauksson and E. Iancu, Jet polarisation in an anisotropic medium, *JHEP* **08** (2023) 027 [[arXiv:2303.03914 \[hep-ph\]](#)].
- [64] M. V. Kuzmin, X. Mayo López, J. Reiten and A. V. Sadofyev, Jet quenching in anisotropic flowing matter, *Phys. Rev. D* **109** (2024) no. 1 014036 [[arXiv:2309.00683 \[hep-ph\]](#)].
- [65] J. Barata, X. Mayo López, A. V. Sadofyev and C. A. Salgado, Medium induced gluon spectrum in dense inhomogeneous matter, *Phys. Rev. D* **108** (2023) no. 3 034018 [[arXiv:2304.03712 \[hep-ph\]](#)].
- [66] J. Barata, C. A. Salgado and J. a. M. Silva, Gluon to $q\bar{q}$ antenna in anisotropic QCD matter: spin-polarized and azimuthal jet observables, [arXiv:2407.04774 \[hep-ph\]](#).
- [67] P. Aurenche and B. G. Zakharov, Parton energy loss in glasma, *Phys. Lett. B* **718** (2013) 937 [[arXiv:1205.6462 \[hep-ph\]](#)].
- [68] J. Barata, S. Hauksson, X. Mayo López and A. V. Sadofyev, Jet quenching in the glasma phase: medium-induced radiation, [arXiv:2406.07615 \[hep-ph\]](#).
- [69] C. Andres, N. Armesto, H. Niemi, R. Paatelainen and C. A. Salgado, Jet quenching as a probe of the initial stages in heavy-ion collisions, *Phys. Lett. B* **803** (2020) 135318 [[arXiv:1902.03231 \[hep-ph\]](#)].
- [70] K. J. Eskola, K. Kajantie, P. V. Ruuskanen and K. Tuominen, Scaling of transverse energies and multiplicities with atomic number and energy in ultrarelativistic nuclear collisions, *Nucl. Phys. B* **570** (2000) 379 [[arXiv:hep-ph/9909456](#)].
- [71] C. Andres, L. Apolinário, F. Dominguez, M. G. Martinez and C. A. Salgado, Medium-induced radiation with vacuum propagation in the pre-hydrodynamics phase, *JHEP* **03** (2023) 189 [[arXiv:2211.10161 \[hep-ph\]](#)].

- [72] S. P. Adhya and K. Tywoniuk, *Sensitivity of jet quenching to the initial state in heavy-ion collisions*, [arXiv:2409.04295 \[hep-ph\]](#).
- [73] D. Zigic, B. Ilic, M. Djordjevic and M. Djordjevic, *Exploring the initial stages in heavy-ion collisions with high- p_{\perp} R_{AA} and v_2 theory and data*, *Phys. Rev. C* **101** (2020) no. 6 064909 [[arXiv:1908.11866 \[hep-ph\]](#)].
- [74] S. Stojku, J. Auvinen, M. Djordjevic, P. Huovinen and M. Djordjevic, *Early evolution constrained by high- p_{\perp} quark-gluon plasma tomography*, *Phys. Rev. C* **105** (2022) no. 2 L021901 [[arXiv:2008.08987 \[nucl-th\]](#)].
- [75] B. Ilic, D. Zigic, M. Djordjevic and M. Djordjevic, *Utilizing high- p_{\perp} theory and data to constrain the initial stages of quark-gluon plasma*, *Int. J. Mod. Phys. E* **30** (2021) no. 11 2141007 [[arXiv:2203.11883 \[hep-ph\]](#)].
- [76] S. K. Das, F. Scardina, S. Plumari and V. Greco, *Toward a solution to the R_{AA} and v_2 puzzle for heavy quarks*, *Phys. Lett. B* **747** (2015) 260 [[arXiv:1502.03757 \[nucl-th\]](#)].
- [77] J. Xu, J. Liao and M. Gyulassy, *Bridging Soft-Hard Transport Properties of Quark-Gluon Plasmas with CUJET3.0*, *JHEP* **02** (2016) 169 [[arXiv:1508.00552 \[hep-ph\]](#)].
- [78] J. Noronha-Hostler, B. Betz, J. Noronha and M. Gyulassy, *Event-by-event hydrodynamics + jet energy loss: A solution to the $R_{AA} \otimes v_2$ puzzle*, *Phys. Rev. Lett.* **116** (2016) no. 25 252301 [[arXiv:1602.03788 \[nucl-th\]](#)].
- [79] S. Cao, L.-G. Pang, T. Luo, Y. He, G.-Y. Qin and X.-N. Wang, *R_{AA} vs. v_2 of heavy and light hadrons within a linear Boltzmann transport model*, *Nucl. Part. Phys. Proc.* **289-290** (2017) 217.
- [80] D. Zigic, I. Salom, J. Auvinen, M. Djordjevic and M. Djordjevic, *DREENA-B framework: first predictions of R_{AA} and v_2 within dynamical energy loss formalism in evolving QCD medium*, *Phys. Lett. B* **791** (2019) 236 [[arXiv:1805.04786 \[nucl-th\]](#)].
- [81] D. Thomas and F. Colamaria, *Recent Findings from Heavy-Flavor Angular Correlation Measurements in Hadronic Collisions*, *Universe* **10** (2024) no. 3 109 [[arXiv:2403.01035 \[nucl-ex\]](#)].
- [82] J. Altmann *et. al.*, *QCD challenges from pp to AA collisions: 4th edition*, *Eur. Phys. J. C* **84** (2024) no. 4 421 [[arXiv:2401.09930 \[hep-ex\]](#)].
- [83] M. Nahrgang, J. Aichelin, P. B. Gossiaux and K. Werner, *Azimuthal correlations of heavy quarks in Pb + Pb collisions at $\sqrt{s} = 2.76$ TeV at the CERN Large Hadron Collider*, *Phys. Rev. C* **90** (2014) no. 2 024907 [[arXiv:1305.3823 \[hep-ph\]](#)].
- [84] J. Zhao, J. Aichelin, P. B. Gossiaux and K. Werner, *System size dependence of energy loss and correlations of heavy mesons at LHC energies*, [arXiv:2407.20919 \[hep-ph\]](#).
- [85] S. Cao, G.-Y. Qin and S. A. Bass, *Dynamical Evolution, Hadronization and Angular De-correlation of Heavy Flavor in a Hot and Dense QCD Medium*, *Nucl. Phys. A* **932** (2014) 38 [[arXiv:1404.1081 \[nucl-th\]](#)].
- [86] F. Scardina, S. K. Das, S. Plumari, D. Perricone and V. Greco, *Heavy Flavor Suppression, Flow and Azimuthal Correlation: Boltzmann vs Langevin*, *J. Phys. Conf. Ser.* **535** (2014) 012019.
- [87] M. Gyulassy and L. McLerran, *New forms of QCD matter discovered at RHIC*, *Nucl. Phys. A* **750** (2005) 30 [[arXiv:nucl-th/0405013](#)].
- [88] L. D. McLerran and R. Venugopalan, *Computing quark and gluon distribution functions for very large nuclei*, *Phys. Rev. D* **49** (1994) 2233 [[arXiv:hep-ph/9309289](#)].
- [89] L. D. McLerran and R. Venugopalan, *Gluon distribution functions for very large nuclei at small transverse momentum*, *Phys. Rev. D* **49** (1994) 3352 [[arXiv:hep-ph/9311205](#)].
- [90] L. D. McLerran and R. Venugopalan, *Green's functions in the color field of a large nucleus*, *Phys. Rev. D* **50** (1994) 2225 [[arXiv:hep-ph/9402335](#)].
- [91] T. Lappi, *Wilson line correlator in the MV model: Relating the glasma to deep inelastic scattering*, *Eur. Phys. J. C* **55** (2008) 285 [[arXiv:0711.3039 \[hep-ph\]](#)].
- [92] K. Fukushima, *Randomness in infinitesimal extent in the McLerran-Venugopalan model*, *Phys. Rev. D* **77** (2008) 074005 [[arXiv:0711.2364 \[hep-ph\]](#)].
- [93] T. Lappi, *Energy density of the glasma*, *Phys. Lett. B* **643** (2006) 11 [[arXiv:hep-ph/0606207](#)].
- [94] H. Fujii and K. Itakura, *Expanding color flux tubes and instabilities*, *Nucl. Phys. A* **809** (2008) 88 [[arXiv:0803.0410 \[hep-ph\]](#)].
- [95] G. Chen and R. J. Fries, *Global Flow of Glasma in High Energy Nuclear Collisions*, *Phys. Lett. B* **723** (2013) 417 [[arXiv:1303.2360 \[nucl-th\]](#)].
- [96] R. J. Fries, *Early Time Evolution of High Energy Heavy Ion Collisions*, *J. Phys. G* **34** (2007) S851 [[arXiv:nucl-th/0702026](#)].
- [97] A. Krasnitz and R. Venugopalan, *Nonperturbative computation of gluon minijet production in nuclear collisions at very high-energies*, *Nucl. Phys. B* **557** (1999) 237 [[arXiv:hep-ph/9809433](#)].
- [98] T. Lappi, *Production of gluons in the classical field model for heavy ion collisions*, *Phys. Rev. C* **67** (2003) 054903 [[arXiv:hep-ph/0303076](#)].
- [99] T. Lappi, *Classical chromodynamics and heavy ion collisions*. PhD thesis, Helsinki U., 2004. [arXiv:hep-ph/0505095](#).
- [100] D. Müller, *Simulations of the Glasma in 3+1D*. PhD thesis, Vienna, Tech. U., 2019. [arXiv:1904.04267 \[hep-ph\]](#).
- [101] S. K. Wong, *Field and particle equations for the classical Yang-Mills field and particles with isotopic spin*, *Nuovo Cim. A* **65** (1970) 689.
- [102] A. D. Boozer, *Classical Yang-Mills theory*, *American Journal of Physics* **79** (2011) no. 9 925.
- [103] U. W. Heinz, *Kinetic Theory for Nonabelian Plasmas*, *Phys. Rev. Lett.* **51** (1983) 351.
- [104] P. F. Kelly, Q. Liu, C. Lucchesi and C. Manuel, *Classical transport theory and hard thermal loops in the quark - gluon plasma*, *Phys. Rev. D* **50** (1994) 4209 [[arXiv:hep-ph/9406285](#)].
- [105] D. F. Litim and C. Manuel, *Effective transport equations for nonAbelian plasmas*, *Nucl. Phys. B* **562** (1999) 237 [[arXiv:hep-ph/9906210](#)].
- [106] D. F. Litim and C. Manuel, *Mean field dynamics in non-Abelian plasmas from classical transport theory*, *Phys. Rev. Lett.* **82** (1999) 4981 [[arXiv:hep-ph/9902430](#)].
- [107] C. R. Hu and B. Muller, *Classical lattice gauge field with hard thermal loops*, *Phys. Lett. B* **409** (1997) 377

- [arXiv:hep-ph/9611292].
- [108] G. D. Moore, C.-r. Hu and B. Müller, *Chern-Simons number diffusion with hard thermal loops*, *Phys. Rev. D* **58** (1998) 045001 [arXiv:hep-ph/9710436].
- [109] A. Dumitru, Y. Nara and M. Strickland, *Ultraviolet avalanche in anisotropic non-Abelian plasmas*, *Phys. Rev. D* **75** (2007) 025016 [arXiv:hep-ph/0604149].
- [110] A. Dumitru and Y. Nara, *Numerical simulation of non-Abelian particle-field dynamics*, *Eur. Phys. J. A* **29** (2006) 65 [arXiv:hep-ph/0511242].
- [111] B. Schenke, M. Strickland, A. Dumitru, Y. Nara and C. Greiner, *Transverse momentum diffusion and jet energy loss in non-Abelian plasmas*, *Phys. Rev. C* **79** (2009) 034903 [arXiv:0810.1314 [hep-ph]].
- [112] H. E. Haber, *Useful relations among the generators in the defining and adjoint representations of $SU(N)$* , *SciPost Phys. Lect. Notes* **21** (2021) 1 [arXiv:1912.13302 [math-ph]].
- [113] A. Andronic *et al.*, *Heavy-flavour and quarkonium production in the LHC era: from proton-proton to heavy-ion collisions*, *Eur. Phys. J. C* **76** (2016) no. 3 107 [arXiv:1506.03981 [nucl-ex]].
- [114] R. Vogt, *Heavy Flavor Azimuthal Correlations in Cold Nuclear Matter*, *Phys. Rev. C* **98** (2018) no. 3 034907 [arXiv:1806.01904 [hep-ph]].
- [115] R. Vogt, *$b\bar{b}$ kinematic correlations in cold nuclear matter*, *Phys. Rev. C* **101** (2020) no. 2 024910 [arXiv:1908.05320 [hep-ph]].
- [116] P. Nason, S. Dawson and R. K. Ellis, *The One Particle Inclusive Differential Cross-Section for Heavy Quark Production in Hadronic Collisions*, *Nucl. Phys. B* **327** (1989) 49. [Erratum: Nucl.Phys.B 335, 260–260 (1990)].
- [117] M. Cacciari, M. Greco and P. Nason, *The p_T spectrum in heavy-flavour hadroproduction.*, *JHEP* **05** (1998) 007 [arXiv:hep-ph/9803400].
- [118] W. Beenakker, W. L. van Neerven, R. Meng, G. A. Schuler and J. Smith, *QCD corrections to heavy quark production in hadron hadron collisions*, *Nucl. Phys. B* **351** (1991) 507.
- [119] I. Helenius and H. Paukkunen, *Revisiting the D -meson hadroproduction in general-mass variable flavour number scheme*, *JHEP* **05** (2018) 196 [arXiv:1804.03557 [hep-ph]].
- [120] M. Cacciari, S. Frixione and P. Nason, *The p_T spectrum in heavy flavor photoproduction*, *JHEP* **03** (2001) 006 [arXiv:hep-ph/0102134].
- [121] P. M. Nadolsky, H.-L. Lai, Q.-H. Cao, J. Huston, J. Pumplin, D. Stump, W.-K. Tung and C. P. Yuan, *Implications of CTEQ global analysis for collider observables*, *Phys. Rev. D* **78** (2008) 013004 [arXiv:0802.0007 [hep-ph]].
- [122] S. Dulat, T.-J. Hou, J. Gao, M. Guzzi, J. Huston, P. Nadolsky, J. Pumplin, C. Schmidt, D. Stump and C. P. Yuan, *New parton distribution functions from a global analysis of quantum chromodynamics*, *Phys. Rev. D* **93** (2016) no. 3 033006 [arXiv:1506.07443 [hep-ph]].
- [123] K. J. Eskola, P. Paakkinen, H. Paukkunen and C. A. Salgado, *EPPS16: Nuclear parton distributions with LHC data*, *Eur. Phys. J. C* **77** (2017) no. 3 163 [arXiv:1612.05741 [hep-ph]].
- [124] M. Abramowitz and I. A. Stegun, *Handbook of Mathematical Functions with Formulas, Graphs, and Mathematical Tables*. Dover, New York, ninth dover printing, tenth gpo printing ed., 1964.
- [125] **Particle Data Group** collaboration, R. L. Workman *et al.*, *Review of Particle Physics*, *PTEP* **2022** (2022) 083C01.
- [126] A. Kurkela, A. Mazeliauskas, J.-F. Paquet, S. Schlichting and D. Teaney, *Effective kinetic description of event-by-event pre-equilibrium dynamics in high-energy heavy-ion collisions*, *Phys. Rev. C* **99** (2019) no. 3 034910 [arXiv:1805.00961 [hep-ph]].
- [127] M. Ruggieri, F. Scardina, S. Plumari and V. Greco, *Thermalization, Isotropization and Elliptic Flow from Nonequilibrium Initial Conditions with a Saturation Scale*, *Phys. Rev. C* **89** (2014) no. 5 054914 [arXiv:1312.6060 [nucl-th]].
- [128] S. Plumari, G. L. Guardo, F. Scardina and V. Greco, *Initial state fluctuations from mid-peripheral to ultra-central collisions in a event-by-event transport approach*, *Phys. Rev. C* **92** (2015) no. 5 054902 [arXiv:1507.05540 [hep-ph]].
- [129] K. J. Golec-Biernat and M. Wusthoff, *Saturation effects in deep inelastic scattering at low Q^2 and its implications on diffraction*, *Phys. Rev. D* **59** (1998) 014017 [arXiv:hep-ph/9807513].
- [130] A. H. Mueller and J.-w. Qiu, *Glueon Recombination and Shadowing at Small Values of x* , *Nucl. Phys. B* **268** (1986) 427.
- [131] K. J. Eskola, H. Paukkunen and C. A. Salgado, *EPS09: A New Generation of NLO and LO Nuclear Parton Distribution Functions*, *JHEP* **04** (2009) 065 [arXiv:0902.4154 [hep-ph]].
- [132] **ALICE** collaboration, *Letter of intent for ALICE 3: A next-generation heavy-ion experiment at the LHC*, arXiv:2211.02491 [physics.ins-det].
- [133] **ATLAS** collaboration, G. Aad *et al.*, *Azimuthal Angle Correlations of Muons Produced via Heavy-Flavor Decays in 5.02 TeV Pb+Pb and pp Collisions with the ATLAS Detector*, *Phys. Rev. Lett.* **132** (2024) no. 20 202301 [arXiv:2308.16652 [nucl-ex]].
- [134] B. Schenke, P. Tribedy and R. Venugopalan, *Fluctuating Glasma initial conditions and flow in heavy ion collisions*, *Phys. Rev. Lett.* **108** (2012) 252301 [arXiv:1202.6646 [nucl-th]].
- [135] S. Schlichting and B. Schenke, *The shape of the proton at high energies*, *Phys. Lett. B* **739** (2014) 313 [arXiv:1407.8458 [hep-ph]].
- [136] H. Mäntysaari, B. Schenke, C. Shen and P. Tribedy, *Imprints of fluctuating proton shapes on flow in proton-lead collisions at the LHC*, *Phys. Lett. B* **772** (2017) 681 [arXiv:1705.03177 [nucl-th]].
- [137] H. Mäntysaari, F. Salazar and B. Schenke, *Nuclear geometry at high energy from exclusive vector meson production*, *Phys. Rev. D* **106** (2022) no. 7 074019 [arXiv:2207.03712 [hep-ph]].
- [138] **CMS** collaboration, V. Khachatryan *et al.*, *Measurement of $B\bar{B}$ Angular Correlations based on Secondary Vertex Reconstruction at $\sqrt{s} = 7$ TeV*, *JHEP* **03** (2011) 136 [arXiv:1102.3194 [hep-ex]].
- [139] **LHCb** collaboration, R. Aaij *et al.*, *Observation of double charm production involving open charm in pp collisions at $\sqrt{s} = 7$ TeV*, *JHEP* **06** (2012) 141 [arXiv:1205.0975 [hep-ex]]. [Addendum: JHEP 03, 108 (2014)].

- [140] **LHCb** collaboration, R. Aaij *et al.*, *Study of $b\bar{b}$ correlations in high energy proton-proton collisions*, *JHEP* **11** (2017) 030 [[arXiv:1708.05994](#) [[hep-ex](#)]].
- [141] **ATLAS** collaboration, M. Aaboud *et al.*, *Measurement of b -hadron pair production with the ATLAS detector in proton-proton collisions at $\sqrt{s} = 8$ TeV*, *JHEP* **11** (2017) 062 [[arXiv:1705.03374](#) [[hep-ex](#)]].
- [142] **ALICE** collaboration, S. Acharya *et al.*, *Azimuthal correlations of prompt D mesons with charged particles in pp and p -Pb collisions at $\sqrt{s_{NN}} = 5.02$ TeV*, *Eur. Phys. J. C* **80** (2020) no. 10 979 [[arXiv:1910.14403](#) [[nucl-ex](#)]].
- [143] **LHCb** collaboration, R. Aaij *et al.*, *Observation of Enhanced Double Parton Scattering in Proton-Lead Collisions at $\sqrt{s_{NN}} = 8.16$ TeV*, *Phys. Rev. Lett.* **125** (2020) no. 21 212001 [[arXiv:2007.06945](#) [[hep-ex](#)]].
- [144] H. Mäntysaari and B. Schenke, *Evidence of strong proton shape fluctuations from incoherent diffraction*, *Phys. Rev. Lett.* **117** (2016) no. 5 052301 [[arXiv:1603.04349](#) [[hep-ph](#)]].
- [145] H. Mäntysaari, *Review of proton and nuclear shape fluctuations at high energy*, *Rept. Prog. Phys.* **83** (2020) no. 8 082201 [[arXiv:2001.10705](#) [[hep-ph](#)]].
- [146] A. Kumar and T. Toll, *Energy dependence of the proton geometry in exclusive vector meson production*, *Phys. Rev. D* **105** (2022) no. 11 114011 [[arXiv:2202.06631](#) [[hep-ph](#)]].
- [147] J. Cepila, J. G. Contreras and M. Krelina, *Coherent and incoherent J/ψ photonuclear production in an energy-dependent hot-spot model*, *Phys. Rev. C* **97** (2018) no. 2 024901 [[arXiv:1711.01855](#) [[hep-ph](#)]].
- [148] S. Demirci and P. Guerrero-Rodríguez, *Evolution of eccentricities induced by geometrical and quantum fluctuations in proton-nucleus collisions*, *Phys. Rev. D* **107** (2023) no. 9 094004 [[arXiv:2302.02236](#) [[hep-ph](#)]].
- [149] C. Bierlich, G. Gustafson, L. Lönnblad and H. Shah, *The Angantyr model for Heavy-Ion Collisions in PYTHIA8*, *JHEP* **10** (2018) 134 [[arXiv:1806.10820](#) [[hep-ph](#)]].
- [150] B. Schenke and S. Schlichting, *3D glasma initial state for relativistic heavy ion collisions*, *Phys. Rev. C* **94** (2016) no. 4 044907 [[arXiv:1605.07158](#) [[hep-ph](#)]].
- [151] D. Gelfand, A. Ipp and D. Müller, *Simulating collisions of thick nuclei in the color glass condensate framework*, *Phys. Rev. D* **94** (2016) no. 1 014020 [[arXiv:1605.07184](#) [[hep-ph](#)]].
- [152] A. Ipp and D. Müller, *Broken boost invariance in the Glasma via finite nuclei thickness*, *Phys. Lett. B* **771** (2017) 74 [[arXiv:1703.00017](#) [[hep-ph](#)]].
- [153] S. Schlichting and P. Singh, *3-D structure of the Glasma initial state – Breaking boost-invariance by collisions of extended shock waves in classical Yang-Mills theory*, *Phys. Rev. D* **103** (2021) no. 1 014003 [[arXiv:2010.11172](#) [[hep-ph](#)]].
- [154] A. Ipp and D. I. Müller, *Progress on 3+1D Glasma simulations*, *Eur. Phys. J. A* **56** (2020) no. 9 243 [[arXiv:2009.02044](#) [[hep-ph](#)]].
- [155] A. Ipp, D. I. Müller, S. Schlichting and P. Singh, *Spacetime structure of (3+1)D color fields in high energy nuclear collisions*, *Phys. Rev. D* **104** (2021) no. 11 114040 [[arXiv:2109.05028](#) [[hep-ph](#)]].
- [156] S. McDonald, S. Jeon and C. Gale, *3+1D initialization and evolution of the glasma*, *Phys. Rev. C* **108** (2023) no. 6 064910 [[arXiv:2306.04896](#) [[hep-ph](#)]].
- [157] H. Matsuda and X.-G. Huang, *Simulation of a (3+1)D glasma in Milne coordinates: Development of the framework*, *Phys. Rev. D* **108** (2023) no. 11 114008 [[arXiv:2308.15269](#) [[hep-ph](#)]].
- [158] A. Ipp, M. Leuthner, D. I. Müller, S. Schlichting, K. Schmidt and P. Singh, *Energy-momentum tensor of the dilute (3+1)D glasma*, *Phys. Rev. D* **109** (2024) no. 9 094040 [[arXiv:2401.10320](#) [[hep-ph](#)]].
- [159] H. Matsuda and X.-G. Huang, *Effect of Longitudinal Fluctuations of 3D Weizsäcker–Williams Field on Pressure Isotropization of Glasma*, *Entropy* **26** (2024) no. 2 167 [[arXiv:2401.04296](#) [[physics.plasm-ph](#)]].
- [160] K. Kajantie, L. D. McLerran and R. Paatelainen, *Gluon Radiation from a Classical Point Particle*, *Phys. Rev. D* **100** (2019) no. 5 054011 [[arXiv:1903.01381](#) [[nucl-th](#)]].
- [161] K. Kajantie, L. D. McLerran and R. Paatelainen, *Gluon Radiation from a classical point particle II: dense gluon fields*, *Phys. Rev. D* **101** (2020) no. 5 054012 [[arXiv:1911.12738](#) [[hep-ph](#)]].
- [162] I. Kolbe and M. Lushozi, *Gluon radiation from a classical point particle: recoil effects*, *Eur. Phys. J. C* **83** (2023) no. 10 886 [[arXiv:2109.01736](#) [[hep-ph](#)]].
- [163] E. V. Shuryak and I. Zahed, *Jet quenching in high-energy heavy ion collisions by QCD synchrotron-like radiation*, *Phys. Rev. D* **67** (2003) 054025 [[arXiv:hep-ph/0207163](#)].
- [164] B. G. Zakharov, *Parton energy loss due to synchrotron-like gluon emission*, *JETP Lett.* **88** (2008) 475 [[arXiv:0809.0599](#) [[hep-ph](#)]].
- [165] M. Li, X. Zhao, P. Maris, G. Chen, Y. Li, K. Tuchin and J. P. Vary, *Ultrarelativistic quark-nucleus scattering in a light-front Hamiltonian approach*, *Phys. Rev. D* **101** (2020) no. 7 076016 [[arXiv:2002.09757](#) [[nucl-th](#)]].
- [166] M. Li, T. Lappi and X. Zhao, *Scattering and gluon emission in a color field: A light-front Hamiltonian approach*, *Phys. Rev. D* **104** (2021) no. 5 056014 [[arXiv:2107.02225](#) [[hep-ph](#)]].
- [167] M. Li, T. Lappi, X. Zhao and C. A. Salgado, *Momentum broadening of an in-medium jet evolution using a light-front Hamiltonian approach*, *Phys. Rev. D* **108** (2023) no. 3 036016 [[arXiv:2305.12490](#) [[hep-ph](#)]].
- [168] J. Berges, K. Boguslavski, S. Schlichting and R. Venugopalan, *Universal attractor in a highly occupied non-Abelian plasma*, *Phys. Rev. D* **89** (2014) no. 11 114007 [[arXiv:1311.3005](#) [[hep-ph](#)]].
- [169] M. Greif, C. Greiner, B. Schenke, S. Schlichting and Z. Xu, *Importance of initial and final state effects for azimuthal correlations in p +Pb collisions*, *Phys. Rev. D* **96** (2017) no. 9 091504 [[arXiv:1708.02076](#) [[hep-ph](#)]].
- [170] A. Dumitru and Y. Nara, *QCD plasma instabilities and isotropization*, *Phys. Lett. B* **621** (2005) 89 [[arXiv:hep-ph/0503121](#)].
- [171] A. Dumitru, Y. Nara, B. Schenke and M. Strickland, *Jet broadening in unstable non-Abelian plasmas*, *Phys. Rev. C* **78** (2008) 024909 [[arXiv:0710.1223](#) [[hep-ph](#)]].

- [172] D. F. Litim and C. Manuel, *Semiclassical transport theory for nonAbelian plasmas*, *Phys. Rept.* **364** (2002) 451 [[arXiv:hep-ph/0110104](#)].
- [173] L. Apolinário, J. Barata and G. Milhano, *On the breaking of Casimir scaling in jet quenching*, *Eur. Phys. J. C* **80** (2020) no. 6 586 [[arXiv:2003.02893](#) [[hep-ph](#)]].